Victor Fidelis

Magnetic Properties of the frustrated J1-J2 square lattice with Kondo interactions

Campo Grande, MS
2026

Victor Fidelis

Magnetic Properties of the frustrated J1-J2 square lattice with Kondo interactions

Final Exam Text to the Institute of Physics of the Federal University of Mato Grosso do Sul as a partial requirement for obtaining the title of Master in Materials Science by the Graduate Program in Materials Science.

Federal University of Mato Grosso do Sul
Physics Institute
Material Sciences Graduate Program

Supervisor: Prof. Dr. Fábio Mallmann Zimmer

Campo Grande, MS
2026

Sumário

Resumo

As propriedades magnéticas e eletrônicas dos materiais são regidas pela complexa interconexão entre interações de troca localizadas e o acoplamento com elétrons itinerantes. Este trabalho investiga a competição entre a frustração magnética e o efeito Kondo em uma rede quadrada $J_1 - J_2$. A frustração magnética é introduzida por interações competitivas entre vizinhos mais próximos (J_1) e segundos vizinhos (J_2). O efeito Kondo, governado pelo acoplamento J_K, introduz um mecanismo de blindagem não magnética através da formação de singletos de Kondo. Para resolver o Hamiltoniano resultante, empregou-se uma aproximação de Campo Médio de Cluster (CMF) acoplada à diagonalização exata em um cluster de 4 sítios. A metodologia é validada pela reprodução do diagrama de fases conhecido do modelo $J_1 - J_2$, demonstrando a supressão da temperatura de Néel (T_N) no ponto de máxima frustração ($J_2/J_1 \approx 0.5$). Os resultados demonstram que a introdução de J_K suprime a ordem magnética de longo alcance, podendo promover a formação de um estado de singleto de Kondo, especialmente no regime de alta frustração. Estes achados caracterizam as fronteiras quânticas entre fases magnéticas e não magnéticas, estabelecendo uma base crucial para o mapeamento do diagrama de fases completo sob diferentes intensidades de acoplamento e densidades eletrônicas.

Palavras-chave: Singleto Kondo, Frustração Magnética, Modelo $J_1 - J_2$, Teoria de Campo Médio de Cluster.

Abstract

The magnetic and electronic properties of materials are governed by the complex interplay between localized exchange interactions and coupling with itinerant electrons. This work investigates the competition between magnetic frustration and the Kondo effect in a $J_1 - J_2$ square lattice. Magnetic frustration is introduced through competing nearest-neighbor (J_1) and next-nearest-neighbor (J_2) interactions. The Kondo effect, governed by the coupling J_K, introduces a non-magnetic screening mechanism via the formation of Kondo singlets. To solve the resulting Hamiltonian, we employ a rigorous Cluster Mean-Field (CMF) approximation coupled with exact diagonalization on a 4-site cluster. The methodology is validated by reproducing the known $J_1 - J_2$ phase diagram, which shows the suppression of the Néel temperature (T_N) at the point of maximum frustration ($J_2/J_1 \approx 0.5$). The results demonstrate that the introduction of J_K further suppresses long-range magnetic order, promoting the formation of a Kondo singlet state, particularly in the highly frustrated regime. These findings characterize the quantum boundaries between magnetic and non-magnetic phases and provide a crucial foundation for mapping the full phase diagram across varying coupling strengths and electron densities.

Keywords: Kondo Singlet, Magnetic Frustration, $J_1 - J_2$ Model, Cluster Mean-Field Theory.

Resumo Expandido

O estudo de sistemas eletrônicos fortemente correlacionados permanece como um dos pilares da física da matéria condensada contemporânea, impulsionado pela vasta gama de fenômenos emergentes que transcendem as descrições de elétrons não interagentes, tais como o magnetismo não convencional, a supercondutividade de alta temperatura e o comportamento de férmions pesados [1]. No âmago desta complexidade, o Modelo de Rede Kondo (KLM) desempenha um papel fundamental ao descrever a interação entre uma banda de condução de elétrons itinerantes e uma matriz periódica de momentos magnéticos localizados. Em sistemas descritos por esse modelo, estabelece-se uma competição intrínseca entre o efeito Kondo, que favorece a formação de singletos locais e a blindagem do momento magnético, e a interação Ruderman-Kittel-Kasuya-Yosida (RKKY), que promove a ordem magnética de longo alcance mediada pelos elétrons de condução. Este equilíbrio competitivo, classicamente descrito pelo cenário de Doniach, define o diagrama de fases e as propriedades fundamentais de materiais de férmions pesados [2]. Entretanto, a paisagem termodinâmica tradicional de Doniach pode ser profundamente alterada quando a geometria da rede ou a natureza das interações de trocas magnéticas introduzem a frustração. Um exemplo típico diz respeito à rede quadrada quando esta apresenta interações além dos spins vizinhos mais próximos. Nessa rede, a coexistência de interações competitivas entre primeiros vizinhos (J_1) e segundos vizinhos (J_2) impede que o sistema satisfaça simultaneamente todas as energias de ligação (para interações antiferromagnéticas), resultando em uma multiplicidade de estados fundamentais quase-degenerados [3]. Embora o modelo $J_1 - J_2$ tenha sido exaustivamente estudado como um protótipo para fases magnéticas induzidas por frustração, variando da fase antiferromagnética de Néel (AF) para a fase de faixas ou stripe (SAF) em torno do ponto crítico $J_2/|J_1| \approx -0,5$, a intersecção simultânea entre a frustração e o efeito Kondo permanece como uma fronteira científica de alta relevância.

Esta dissertação aborda essa lacuna investigando o Modelo de Rede Kondo na rede quadrada $J_1 - J_2$, tratando a frustração como um parâmetro de ajuste

secundário que atua em conjunto com o acoplamento Kondo. O problema torna-se particularmente sutil ao considerar como as flutuações quânticas intensificadas pela frustração podem facilitar ou inibir a transição para o estado de férmion pesado. Compreender como o preenchimento eletrônico (n) influencia a robustez dessas fases magnéticas e a natureza das transições de fase é essencial não apenas do ponto de vista teórico, mas também para o design de novos materiais com propriedades magnéticas "sintonizáveis".

A investigação das propriedades magnéticas e de transporte deste sistema fundamenta-se no Hamiltoniano do Modelo de Rede Kondo estendido, definido em uma rede quadrada com N sítios. O modelo é composto por três termos principais: a energia cinética dos elétrons de condução, descrita por um termo de hopping (t) entre primeiros vizinhos; a interação de troca local de Kondo (J_K), que acopla o spin dos elétrons itinerantes aos momentos locais $S = 1/2$; e o termo de troca magnética entre os spins localizados, que incorpora as interações J_1 e J_2que podem induzir frustração. Isso permite explorar a transição entre a ordem antiferromagnética de Néel e a fase de faixas (stripes).

Para transpor as limitações das teorias de campo médio de sítio único, que negligenciam correlações espaciais e flutuações quânticas locais cruciais em sistemas frustrados, este trabalho emprega a Teoria de Campo Médio de Aglomerados (Cluster Mean-Field - CMF). A metodologia consiste em particionar a rede infinita em aglomerados idênticos de tamanho finito, especificamente, grupos de 2×2 sítios (4 sítios). Dentro de cada aglomerado, todas as interações de muitos corpos são tratadas de forma exata via Diagonalização Exata (ED), preservando as flutuações quânticas internas. A conectividade com o restante da rede é restabelecida através de campos médios auto-consistentes que agem nas fronteiras do aglomerado, representando a ordem magnética de longo alcance e a hibridização efetiva.

O desafio computacional reside na dimensão do espaço de Hilbert, que para um aglomerado de 4 sítios com 4 elétrons, atinge 1120 estados, ($2^4 \cdot \frac{(8)!}{(8-4)!4!}$, onde 2^4 é a contagem os estados dos sítios e a fração, de distribuição eletrônica). Para otimizar a solução numérica, foi implementado um algoritmo em linguagem *Fortran* utilizando máscaras de bits (bitwise operations) para representar as configurações de spin e ocupação eletrônica. O procedimento iterativo busca a convergência

dos parâmetros de ordem (magnetizações das sub-redes) e da energia livre do sistema. Através desta abordagem, foi possível calcular o diagrama de fases global em função da temperatura (T), da intensidade do acoplamento Kondo e da razão de frustração $J_2/|J_1|$, permitindo uma análise precisa da estabilidade das fases magnéticas frente ao aumento do preenchimento eletrônico.

Os resultados obtidos revelam uma competição complexa entre as ordens magnéticas e a blindagem Kondo, modulada pela competição entre J_1 e J_2 na rede e pela densidade de portadores. No regime de preenchimento parcial ($n = 1$), o diagrama de fases exibe as transições clássicas do modelo J_1-J_2. Para valores baixos de J_K, a fase antiferromagnética de Néel (AF) domina a região onde $J_2/|J_1| > -0,5$. Com o aumento da frustração ($J_2/|J_1| \to -0,5$), observa-se a transição para a fase de faixas (stripe ou SAF), caracterizada por vetores de onda de ordenamento distintos. A introdução do acoplamento J_K atua como um mecanismo de supressão dessas ordens. Para valores suficientemente elevados de J_K, o sistema transita para uma fase de Singleto Kondo, onde os momentos locais são blindados pelos elétrons de condução, resultando em um estado não magnético de férmions pesados.

Um dos achados mais significativos desta pesquisa é a dependência do diagrama de fases em relação ao n. Observou-se que a estabilidade das fases magnéticas é drasticamente alterada quando o sistema é afastado do regime de baixo preenchimento. Em densidades eletrônicas baixas, a eficácia do efeito Kondo é reduzida devido à escassez de elétrons disponíveis para realizar a blindagem dos spins localizados, o que permite que a ordem magnética persista mesmo para valores de J_K que, em $n = 4$, seriam suficientes para colapsar o ordenamento. Além disso, a análise da energia livre e dos parâmetros de ordem sugere que a frustração atua de forma sinérgica com J_K na desestabilização da ordem de Néel, facilitando a emergência do estado paramagnético em regiões onde a competição entre as interações magnéticas já enfraqueceu a rigidez da sub-rede.

A investigação das magnetizações de sub-rede revelou ainda que a transição entre as fases AF e SAF é sensível à flutuação quântica capturada pelo aglomerado de 2×2 sítios. Ao contrário de abordagens de campo médio simples, o método Cluster Mean-Field permitiu identificar que o ponto de máxima frustração ($J_2/|J_1| \approx -0,5$) funciona como uma "janela" de instabilidade magnética, onde o efeito Kondo torna-se mais pronunciado. Este comportamento é evidenciado pela

redução da temperatura crítica (T_c) e pelo aumento da hibridização efetiva, sugerindo que materiais reais que operam próximos a este ponto crítico podem exibir propriedades de transporte anômalas e comportamento de líquido de Fermi não convencional.

As conclusões desta dissertação reiteram a complexidade inerente ao Modelo de Rede Kondo em redes frustradas e oferecem uma visão detalhada sobre como a frustração e o preenchimento eletrônico modulam a competição de Doniach. A principal contribuição deste estudo reside na demonstração de que a frustração magnética não apenas desestabiliza as ordens de longo alcance, mas também atua como um catalisador para a formação do estado de Singleto Kondo em densidades eletrônicas específicas. Este fenômeno sugere que a manipulação da geometria da rede e do dopagem de portadores são ferramentas eficazes para controlar a transição entre estados magnéticos ordenados e fases de férmions pesados com alta massa efetiva.

Do ponto de vista da Ciência dos Materiais, os resultados obtidos fornecem uma base teórica para a interpretação de comportamentos anômalos observados em compostos intermetálicos de terras-raras e actinídeos, onde a estrutura cristalina impõe restrições aos spins locais. A identificação de uma "janela de oportunidade" para o efeito Kondo próximo ao ponto de transição $J_2/|J_1| \approx -0,5$ abre caminho para o estudo de pontos críticos quânticos induzidos por frustração, onde a supressão da temperatura de ordenamento magnético pode dar origem a estados de líquido de Fermi não convencional e até mesmo supercondutividade mediada por flutuações de spin.

Finalmente, este trabalho estabelece as bases para investigações futuras que incluam o efeito de campos magnéticos externos e a análise da condutividade, o que permitiria uma comparação direta com dados experimentais. Sugere-se também a expansão do método Cluster Mean-Field para aglomerados maiores a fim de explorar a fase de isolante Kondo.

1 Introduction

The study of strongly correlated electronic systems has been a vibrant topic in condensed matter physics, primarily due to the rich variety of phenomena they exhibit, such as magnetism, superconductivity, and heavy fermion behavior [4–6]. Among these phenomena, the emergence of complex magnetic phases due to frustration and the Kondo effect has garnered significant attention. Central to this complexity is the Kondo Lattice Model, which describes the interaction between conduction electrons and a periodic array of localized magnetic moments. In these systems, a fundamental competition arises between the Kondo screening of local moments by conduction electrons and the Ruderman-Kittel-Kasuya-Yosida (RKKY) interaction which promotes long-range magnetic order [6], this competition is known as the Doniach scenario.

However, the traditional Doniach landscape is significantly altered when the underlying lattice geomety or the nature of exchange interactions introduce frustration. In the square lattice, the competition between nearest-neighbor (J_1) and next-nearest-neighbor (J_2) interactions prevents the from satisfying all bond energies simultaneously, leading to a rich variety of ground states and magnetic phases [7, 8], including Néel antiferromagnetism and stripe (collinear) phases.

An interesting perspective for analyzing frustrated systems can be given by the Ising model, which considers interactions between localized spins on vertices of a lattice. When this model considers the localized moments on a square lattice with exchange interactions between first-neighbors (J_1) and second-neighbors (J_2), a competition can occur, leading to frustration [7]. This model is called the $J_1 - J_2$ Ising model on a square lattice and has been extensively studied as a prototypical system for understanding frustration-induced magnetic phases.

Despite extensive research into frustrated magnetism and the Kondo effect independently, the simultaneous presence of exchange frustration and Kondo screening remains an open question of high theoretical significance. Specifically, how frustration modifies the quantum critical points where magnetism vanishes in favor of a Heavy Fermion state is a problem that requires sophisticated numerical tre-

atments. This dissertation addresses this gap by investigating the $J_1 - J_2$ Kondo Lattice Model on a square lattice, focusing on how frustration acts as a secondary tuning parameter alongside the Kondo coupling.

1.1 Objectives

The primary objective of this work is to determine the magnetic an thermodynamic properties of the frustrated J_1-J_2 square lattice interacting with a conduction band via Kondo coupling. To achieve this we aim to:

- Map the phase diagram by identifying the boudaries between antiferromagnetic (AF), Stripe Antiferromagnetic (SAF), and Paramagnetic (PM) phases as functions of the frustration ratio ($J_2/|J_1|$), Kondo coupling strength (J_K), and conduction electron density (n).
- Analyze transition orders by utilizing free-energy calculations to distinguish between continuous phase transitions (second-order) and discontinuous transitions (first-order). Specifically, investigate how the electron filling n influences the "abruptness" of these transitions in the vicinity of the frustration-induced quantum critical point.
- Characterize the Competition of Energy Scales by systematically evaluate how the interplay between the Kondo energy scale and the exchange interactions (J_1, J_2) governs the stability of the magnetic phases. Specifically, investigate how frustration-induced fluctuations facilitate the transition into the non-magnetic Kondo singlet state, providing insights into the design of heavy-fermion materials with tunable magnetic properties.

1.2 Methodology

The model $J_1 - J_2$ is adopted to describe the magnetic interactions between localized moments on a square lattice, with the possibility of Kondo coupling between itinerant electrons and localized moments. This $J_1 - J_2$ model with Kondo interaction must be treated by dividing the lattice into identical clusters with four

sites each. For the itinerant part, it is proposed to restrict the hopping term to sites belonging to the same cluster, in competition with the Kondo interaction.

The magnetic interactions between clusters are treated within a mean-field approximation, while the interactions within each cluster are calculated exactly using numerical diagonalization techniques.

For this model, the partition function and the thermodynamic potential are obtained, from which different quantities and observables can be derived.

The effective model is then solved self-consistently, where the mean-field of a single cluster solved exactly by numerical diagonalization methods.

Thus, the interaction between clusters is treated at the mean-field level, while the resulting dynamics of intra-cluster interactions is considered exactly, including exchange interactions between localized moments, Kondo interaction, and the hopping term of itinerant electrons.

To treat the many-body nature of the Hamiltonian, we employ the Cluster Mean-Field (CMF) approximation. Unlike standard Mean-Field Theory, which replaces all neighbors with a static average, CMF treats a finite cluster of sites (in this case, a 2×2 plaquette) with exact diagonalization. This preservation of local quantum fluctuations is essential in frustrated systems, where the local topology of the J_1 and J_2 bonds dictates the stability of the macroscopic phase. The inter-cluster interactions are then handled self-consistently, allowing us to probe the thermodynamic limit while maintaining the integrity of the frustrated local environment.

The analysis of the results is performed through graphs showing the behavior of spin correlations for various configurations of exchange interactions, Kondo interaction, and itinerant electron density, both in the ground state and at finite temperature. Local magnetizations are also analyzed, allowing for the construction of phase diagrams to evaluate the competition between possible states: paramagnetic, antiferromagnetic, striped and Kondo singlet formation.

1.3 Organization of the Work

This dissertation is structured to provide a logical progression from the fundamental theory of magnetism and the Kondo effect to the specific numerical results

of the $J_1 - J_2$ Kondo Lattice Model. The chapters are organized as follows:

- **Chapter 2: Theoretical Background:** Establishes the physical foundation of the work. It reviews the principles of quantum magnetism, the $J_1 - J_2$ Heisenberg model on a square lattice, and the physics of the Kondo effect. Special attention is given to the Doniach scenario and the concept of geometric frustration.

- **Chapter 3: Model:** Introduces the specific Hamiltonian used to describe the $J_1 - J_2$ Kondo Lattice Model and discuss the physical parameters that define the phase space of the system.

- **Chapter 4: Numerical Procedures:** Describes the implementation the the Cluster Mean-Field Theory. It details the exact diagonalization method used for intra-cluster interactions and the self-consistent cycle for inter-cluster mean-field, and the thermodynamic observables such as correlation functions and free energy.

- **Chapter 5: Results and Discussion:** Presents the core findings of this research. This includes the benchmark results for the J_1-J_2 model without Kondo coupling, followed by the evolution phase diagrams obtained as Kondo strengthen and the analysis of the suppression of the Néel and Stripe phases and characterize the nature of the resulting phase transitions.

- **Chapter 6: Conclusion:** Synthesizes the primary findings of this research, specifically addressing the competitive interplay between exchange frustration and Kondo screening. It provides a final analysis of how the conduction electron density dictates the resilience of magnetic phases and governs the vanishing of first-order transition boundaries, a result of significant interest for the design of heavy-fermion materials. The chapter concludes with a discussion on the limitations of the current cluster approximation and proposes future directions for probing quantum critical regimes and potential spin-liquid states.

2 Theoretical Background

When exploring magnetic frustration, two types comes to mind: geometric frustration, which arises from the lattice geometry, and exchange frustration, which occurs due to competing interactions of different signs or magnitudes. Regardless of the type of frustration, a frustrated system is characterized by a large number of nearly degenerate ground states, which can pair with other interactions and give rise to quantum phases. In addition, the presence of the Kondo effect in magnetic materials can influence magnetic ordering as well as transport phenomena, providing a fruitful platform for exploring new physical properties.

An investigation into the quantum phases of the J_1-J_2 Kondo model requires a detailed understanding of the fundamental mechanisms. This chapter reviews the essential theoretical concepts that form the basis of the present work. We begin by examining the concepts of magnetism, magnetic models, introduction of the physics of quantum magnetism, frustration, the Kondo effect, and the interplay between magnetic order and the Kondo effect.

This background is crucial and provides the foundation for the issues explored in this study.

2.1 Magnetism

Magnetism is a fundamental property of matter, resulting from the quantum mechanical properties of electrons. Every localized electron possesses both an orbital angular momentum due to its motion around the atomic nucleus and an intrinsic spin angular momentum [9, 10]. These angular momenta are from the electron's charge and generate corresponding magnetic dipole moments. Within an atom, the combination of these individual electronic moments, based on principles like Hund's rules and the exclusion principle, can lead to a net atomic magnetic moment, particularly pronounced in atoms with partially filled d or f electron shells. These localized atomic moments serve as the building blocks for all macroscopic magnetic phenomena.

2.1.1 Classical Magnetism vs Quantum Magnetism

Before delving into the quantum mechanical origins of magnetism, it is instructive to consider the classical perspective. In classical physics, magnetism arises from moving electric charges, which generate magnetic fields according to Maxwell's equations [10]. A simple example is a current-carrying wire, where the motion of electrons creates a magnetic field encircling the wire. Similarly, in macroscopic magnets, the alignment of microscopic magnetic dipoles (which can be thought of as tiny current loops) leads to a net magnetic field.

In the framework of classical electromagnetism, magnetism is often treated as the magnetic response of a material to an external magnetic field ($\mathbf{H}$). This response is characterized by quantities such as magnetization (M) and magnetic susceptibility (χ), which describe how a material becomes magnetized in the presence of an applied magnetic field [11]. However, a purely classical treatment of a system of charged particles in thermal equilibrium predicts no net magnetization, as stated by the Bohr-van Leeuwen theorem [9]. Consequently, magnetism cannot be fully explained without invoking quantum mechanics.

The transition from classical to quantum-statistical magnetism involves replacing the continuous classical trajectories of particles with discrete quantum states and accounting for the Pauli Exclusion Principle. This leads to the emergence of the exchange interaction J, which is several orders of magnitude stronger than classical dipole-dipole interactions and is responsible for the alignment of spins in magnetic materials [9,10]. While classical thermodynamics can describe the phase transition at Curie temperature (T_c) through phenomenological models like Landau Theory [12], the microscopic justification for the parameters in those models (such as the discrete state on the Ising model and the isotropic Heisenberg model) comes from quantum mechanics.

2.1.2 Magnetic interactions

The vast array of magnetic behaviors observed in materials, ranging from paramagnetism to the more complex ordered states like ferromagnetism and antiferromagnetism, is primarily determined by the interactions between these elementary magnetic moments [6, 9]. Unlike classical dipole-dipole interactions, which

are generally weak and long-range, the dominant forces aligning spin in solids are fundamentally quantum mechanical in origin and are collectively known as exchange interactions. These short-range interactions dictate the alignment or anti-alignment of electron spins and, the macroscopic magnetic properties. A thorough understanding of these exchange mechanisms is crucial for comprehending the magnetic phenomena of materials.

One primary type of exchange interaction is the Direct Exchange Interaction, which arises from the direct Coulomb interaction of electrons on adjacent ions. It is a short-range, highly directional interaction, typically dominant in materials where the wave functions overlap which means their atoms are significantly closer. This mechanism is responsible for the strong ferromagnetic or antiferromagnetic coupling observed in many elemental metals (e.g., Fe, Ni, Co) and insulators (e.g., MnO) [9].

In contrast, in many metallic diluted alloys or intermetallic compounds, localized magnetic moments are too far apart for direct exchange interaction to be effective. In these cases, the interaction between localized moments is mediated indirectly by the itinerant conduction electrons of the host metal. An example of this is the Ruderman-Kittel-Kasuya-Yosida (RKKY) interaction [6, 13–15]. In the RKKY mechanism, a localized magnetic moment align the spins of the surrounding conduction electrons via the $s-d$ exchange interaction. These polarized conduction electrons then propagate through the crystal, interacting with and polarizing other distant localized magnetic moments. The RKKY interaction is oscillatory in nature, meaning its sign (ferromagnetic or antiferromagnetic coupling) and magnitude oscillate with the distance between the magnetic moments.

The $s-d$ exchange interaction, which forms the basis for the Kondo effect, describes the local coupling between the spin of a localized magnetic impurity (often an unfilled d or f shell) and the spin of the itinerant conduction electrons in the host metal [6]. While the RKKY interaction describes the indirect coupling between two distant impurity spins mediated by conduction electrons, the $s-d$ exchange is the fundamental local interaction between an impurity and the surrounding conduction electrons that drives both RKKY and the Kondo effect. In the context of the Kondo effect, this $s-d$ interaction is typically antiferromagnetic, meaning the impurity spin attempts to align antiparallel to the conduction

electron spins, leading to a dynamic screening phenomenon at low temperatures.

Ultimately, the macroscopic magnetic response of a material to an external magnetic field is quantitatively characterized by its total magnetization (M) and magnetic susceptibility (χ). Magnetization is the net magnetic dipole moment per unit volume of the material, expressed in the International System in units of Amperes per meter (Am^{-1}), and is a vector quantity reflecting the collective alignment of atomic moments within the material [9]. It quantifies the collective magnetic alignment of atomic moments within the material, and also gives insight into the response of the system to external magnetic fields as well as how the material changes the magnetic field. The magnetization M is typically measured as a function of both the applied magnetic field (H) and temperature (T), yielding $M(H, T)$ curves that reveal information about the nature of magnetic ordering, phase transitions, and the strength of underlying exchange interactions.

Magnetic susceptibility (χ) is a dimensionless quantity that quantifies the degree to which a material becomes magnetized in response to an applied magnetic field. It is the ratio of magnetization to the applied magnetic field, $\chi = M/H$ [10]. Susceptibility measurements are particularly powerful in distinguishing different magnetic characteristics: diamagnetic materials exhibit a small, negative susceptibility, while paramagnetic materials show a small, positive susceptibility. In magnetically ordered systems, the temperature dependence of susceptibility can reveal critical temperatures for transitions (e.g., Curie temperature for ferromagnets, Néel temperature for antiferromagnets). Careful analysis of $M(H, T)$ and $\chi(T)$ data allows for the experimental determination of the type and strength of the underlying exchange interactions.

2.1.3 Magnetic Models

2.1.3.1 Ising Model

The Ising model is one of the simplest and most studied models in statistical mechanics and condensed matter physics. It consists of discrete variables called spins, which can take on one of two values, $+1$ and -1, representing "up" and "down" states along a specific axis. The spins are arranged on a lattice, and each spin interacts with its nearest neighbors [9, 16]. The Hamiltonian of the Ising

model is given by

$$H = -J \sum_{\langle i,j \rangle} S_i S_j - h \sum_i S_i, \tag{2.1}$$

where J is the exchange interaction between neighboring spins, S_i and S_j are the spin variables at sites i and j, $\langle i, j \rangle$ denotes that the sum is over nearest-neighbor pairs, and h is an external magnetic field. The first term represents the interaction energy between neighboring spins, while the second term accounts for the influence of an external magnetic field.

Here, the effects of the dimensionality and lattice structure on the magnetic properties of the system can be studied. The Ising model exhibits no phase transition in one dimension [16], while in two dimensions, it shows a phase transition at a finite temperature, known as the critical temperature T_c. The exact solution for the two-dimensional Ising model without an external magnetic field was provided by Lars Onsager in 1944 [17]. The structure of these two lattices is illustrated in Fig. 1, where the nearest-neighbor sites are shown for the one- and two-dimensional lattices.

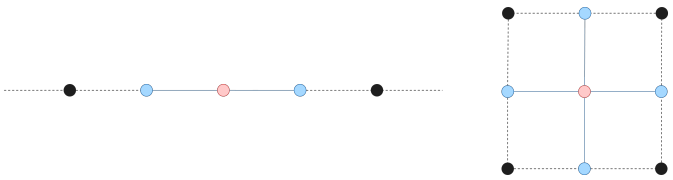

Figure 1 – Nearest-neighbors (blue) of a site (red) in a 1D (left) and 2D (right) lattice. In 1D, each spin has two nearest-neighbors, while in 2D, each spin has four nearest-neighbors. Source: Author.

A generalization of the Ising model is the inclusion of interactions beyond nearest-neighbors, such as next-nearest-neighbors, shown in Eq. 2.2, where a spin in site i can interact with both it's immediate neighbor mediated by J_1, and it's neighbors' neighbor mediated by J_2. This leads to more complex behavior and can introduce frustration, as will be discussed in section 2.1.4.

$$H = -J_1 \sum_{\langle i,j \rangle} S_i S_j - J_2 \sum_{\langle\langle i,k \rangle\rangle} S_i S_k - h \sum_i S_i \tag{2.2}$$

2.1.3.2 Heisenberg Model

While the Ising model provides valuable insights into magnetic systems, it is limited to spins that can only point up or down along a specific axis. The Heisenberg model generalizes this concept by allowing spins to be isotropic in space. The Hamiltonian of the Heisenberg model is given by

$$H = -\sum_{\langle i,j \rangle} J_{ij} \mathbf{S}_i \cdot \mathbf{S}_j, \tag{2.3}$$

where J_{ij} is the exchange interaction between spins at sites i and j, and $\mathbf{S}_i$ and $\mathbf{S}_j$ are the spin operators at those sites. The dot product $\mathbf{S}_i \cdot \mathbf{S}_j$ accounts for the full vector nature of the spins, allowing for a more realistic description of magnetic interactions.

While the Mermin-Wagner theorem [18] precludes long-range order in the isotropic 2D limit, the Cluster Mean-Field approach employed in this work yields finite transition temperatures. These results should be understood as indicating the robust development of magnetic correlations rather than a violation of the theorem.

2.1.3.3 Quantum Formalism and the Hilbert Space

A rigorous treatment of magnetic Hamiltonians requires the formalism of quantum mechanics, where the state of a system is described within a many-body Hilbert space $\mathcal{H}$. For a lattice of N localized spins, each with spin quantum number S, the local Hilbert space of each site i is (2S+1)-dimensional. The total Hilbert space of the system is the tensor product $\mathcal{H} = \bigotimes_{i=1}^{N} \mathcal{H}_i$, resulting in a total dimension of $(2S+1)^N$ [19].

In this space, the spin variables S_i are represented as Hermitian operators, $\hat{S}_i = (\hat{S}_i^x, \hat{S}_i^y, \hat{S}_i^z)$, that obey the angular momentum commutation relations:

$$[\hat{S}_i^\alpha, \hat{S}_j^\beta] = i\hbar\delta_{ij}, \tag{2.4}$$

where δ_{ij} is the Kronecker delta.

This mathematical structure defines the quantum nature of the system. For a single site i, if the spin is measured along the x-direction and then the y-direction,

the act of measuring the second disrupts the first. This non-commutativity is closely tied to the uncertainty principle for angular momentum [20].

In quantum mechanics, if two identical electrons at positions $\mathbf{r}_1$ and $\mathbf{r}_2$ with spins σ_1 and σ_2 are exchanged, the total wave function $\Psi(1,2)$ must be antisymmetric, due to the fermionic nature of electrons. This means if two particles are swapped (exchange), the wave function must change sign:

$$\Psi(\mathbf{r}_1, \sigma_1; \mathbf{r}_2, \sigma_2) = -\Psi(\mathbf{r}_2, \sigma_2; \mathbf{r}_1, \sigma_1). \tag{2.5}$$

This requirement for antisymmetry (Pauli Exclusion Principle) creates an effective force called the exchange interaction. The spatial symmetry of the wave function is linked to the spin symmetry. If the spatial part is symmetric, the spin part must be antisymmetric, forming a singlet state. And if the spatial part is antisymmetric, the spin part must be symmetric, forming a triplet state [9].

The energy difference between singlet and triplet states leads to the exchange interaction, $J = E_s - E_t$, where E_s and E_t correspond to the singlet and triplet energies, respectively. When the spatial overlap of the wave functions favors the antisymmetric spatial state (triplet), due to minimized Coulomb repulsion, the exchange interaction is positive ($J > 0$), leading to ferromagnetic coupling. Conversely, if the symmetric spatial state (singlet) is favored, the exchange interaction is negative ($J < 0$), resulting in antiferromagnetic coupling [9, 16].

While the fundamental interactions are quantum mechanical, modeling many-body magnetic systems often relies on simplified yet powerful effective Hamiltonians. The Heisenberg model, Eq. (2.3), is commonly employed in this regard, describing a lattice of interacting spins quantum mechanically. In the model (2.3), J_{ij} is the exchange coupling constant between the quantum spin operators at sites i and j [9, 12]. Furthermore, this model can capture both ferromagnetic ($J_{ij} > 0$) and antiferromagnetic ($J_{ij} < 0$) interactions.

An interesting simplification of the Heisenberg model is by assuming a strong spin anisotropy. This simplification can lead to the Ising model, which is also given by the Hamiltonian

$$H = -\sum_{\langle i,j \rangle} J_{ij} S_i^z S_j^z, \tag{2.6}$$

in which the spins are restricted to point only along a specific axis, e.g. z, represented by $S_i^z = \pm 1$ [9]. Despite its apparent simplicity, the Ising model has been instrumental in understanding the fundamental physics of phase transitions, critical phenomena, and cooperative behavior in magnetic systems, offering insights into how microscopic interactions lead to macroscopic ordered states [2, 21]. Particularly, the spin operators of the Ising model commute: $[\hat{S}_i^z, \hat{S}_j^z] = 0$.

2.1.4 Frustration

Another intriguing phenomenon in magnetism regards frustration. Frustration, in this context, refers to the inability of a magnetic lattice to find a single ground state in which the energy is minimized, leading to multiple degenerate or nearly degenerate configurations with energy higher than the absolute minimum [16].

Geometric frustration arises from the lattice structure itself, where the arrangement of spins on lattice sites is incompatible with the preferred interactions between them. The canonical example of geometric frustration is the antiferromagnetic Ising model on a triangular lattice. In this case, each spin prefers to be anti-aligned with its neighbors, but due to the triangular arrangement, it is impossible for all three spins in a triangle to be anti-aligned simultaneously, leading to frustration and a degenerate ground state [22].

To illustrate this phenomenon, Fig. 2 shows a triangular plaquete with three spins interacting antiferromagnetically. If two spins, (a) and (b), align antiparallel, the third spin (c) cannot simultaneously be antiparallel to both of them, as shown in the left panel of Fig. 2. This geometric constraint, combined with antiferromagnetic interactions, leads to frustration, as no configuration can satisfy all pairwise interactions [16].

This arrangement leads to a situation where exact one bond in the triangle cannot be satisfied, resulting in a frustrated system with a highly degenerate ground state, as illustrated in the right panel of Fig. 2, with six of the eight possible spin states being degenerated.

This lack of a unique ground state enhances quantum fluctuations, which is a necessary condition for the emergence of exotic magnetic phases, such as spin liquids. In these states, the spins remain disordered and entangled even as $T \to 0$

[1, 16]. However, it is important to note that frustration alone does not ensure a spin liquid; for instance, the isotropic Heisenberg model on a nearest-neighbor triangular lattice typically settles into a non-collinear 120° ordered state.

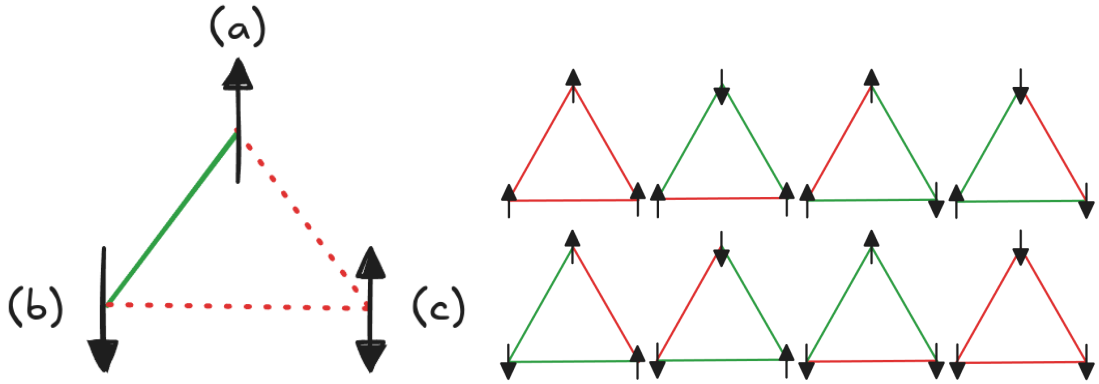

Figure 2 – In the left panel, antiferromagnetic interactions on a triangular lattice lead to frustration, as not all spins can be anti-aligned simultaneously. If spin (a) is up and spin (b) is down, spin (c) cannot be antiparallel to both, leading to frustration in the triangular lattice. The right panel exhibited the eight possible spin configurations. Source: Author.

An interesting situation can arise when isotropic spins are considered. The continuous nature of the Heisenberg model also changes the system's response to frustration. In the antiferromagnetic Ising model on a triangular lattice, for example, the ground state is highly degenerate due to frustration, and colinear. However, Heisenberg spins can adopt non-colinear arrangements, such as the 120-degree structure, which alleviates frustration and leads to a unique ground state [16]. This ability to tilt spins allows the system to satisfy all bonds partially, Figure 3 illustrates this concept.

It is important to remark that frustration is also present in other lattice geometries, including the kagomé lattice and three-dimensional structures such as the pyrochlore lattice, as illustrated in Fig. 4. For instance, the kagome lattice, which consists of corner-sharing triangles, can also exhibit frustration due to the triangular arrangements of spins, leading to a highly degenerate ground state and complex magnetic behavior [24]. Those degenerate ground states can be observed due to the presence of a non-zero residual entropy as temperature approaches

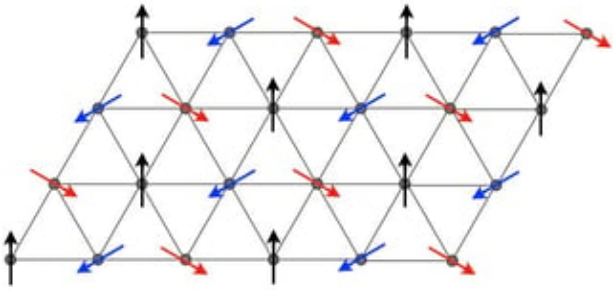

Figure 3 – In the Heisenberg model on a triangular lattice, spins can adopt a 120-degree arrangement (right) to partially satisfy all antiferromagnetic interactions, reducing frustration compared to the colinear arrangement (left) in the Ising model. Source: [23].

zero, indicating that the system retains a finite amount of disorder even at absolute zero [22].

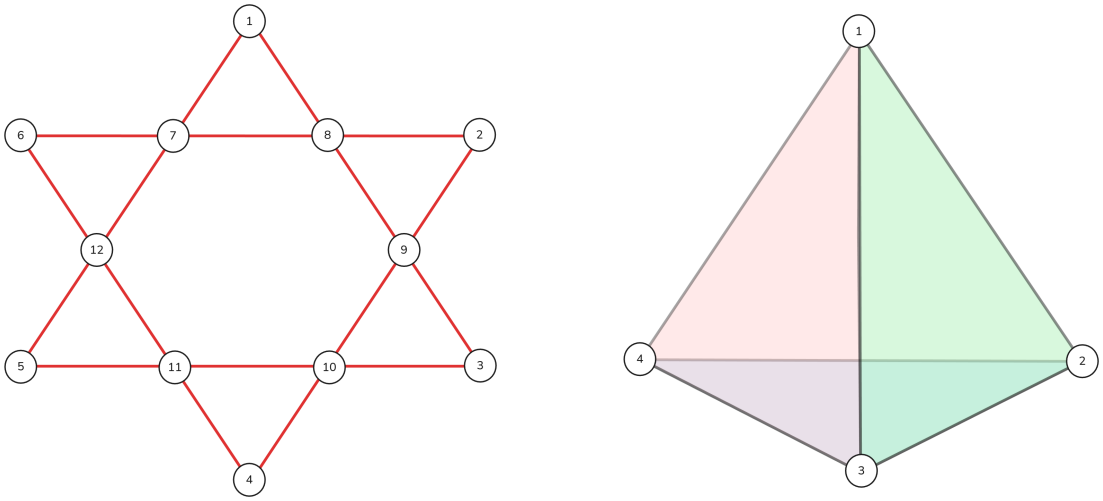

Figure 4 – Two unit structures, one from a Kagomé lattice on the left side and another from a pyroclhore structure on the right. Both are geometric frustrated entities. Source: Author.

Another way to introduce frustration is by considering different exchange interactions, as in the square lattice with nearest-neighbor (J_1) and next-nearest-neighbor (J_2). An illustration of these interactions is provided in Fig. 5, which shows a square-lattice plaquette with four sites and their respective interactions. In this case, when both J_1 and J_2 are antiferromagnetic interactions (or $J_1 > 0$

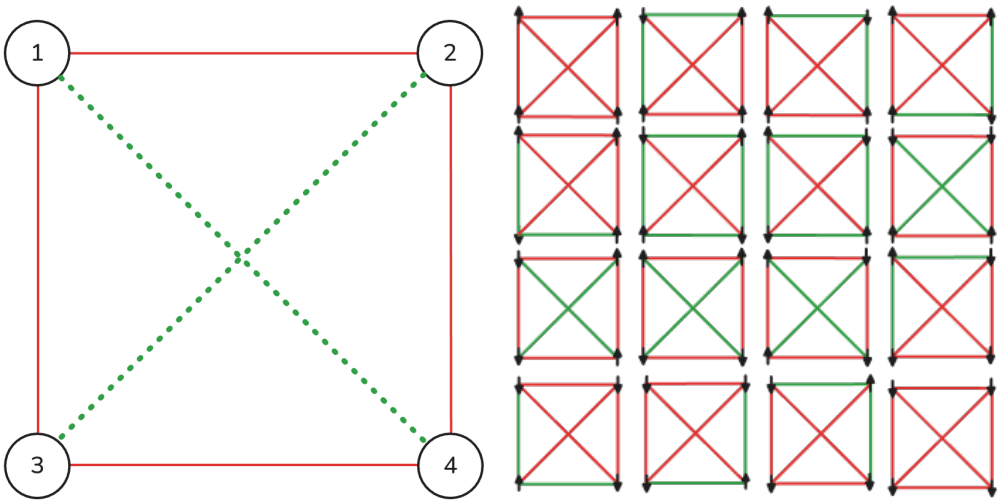

Figure 5 – For the left image red continuous line represent first neighbor interactions (J_1), and green doted line is the second neighbor interactions (J_2). For the right image the arrows indicates the spins orientations, red lines indicates alignment and green lines, anti-alignment. Source: Author.

with $J_2 < 0$) a conflict situation can occur. For instance, when J_2 is sufficiently strong relative to J_1, the system cannot satisfy both interactions simultaneously, leading to a frustrated state [16]. On the other hand, a non-frustrated situation occurs in the absence of second-neighbor interactions ($J_2 = 0$), in which all interactions can be satisfied, for example, by the arrangement with spins 1 and 3 pointing up and spins 2 and 4 pointing down.

A very notable side effect of frustration is the expected suppression of phase transition temperatures. For the Ising J_1-J_2 model, the expected behavior is the decrease of the critical temperature (T_c) as the next-nearest-neighbor interaction (J_2) increases in magnitude relative to the nearest-neighbor interaction (J_1), presenting a minimum temperature when the ratio $J_2/|J_1|$ approaches -0.5, where the frustration is maximized, after that the system changes to the striped phase (SAF) [7].

2.2 Kondo Effect

The previously discussed models (Ising, Heisenberg) primarily focus on insulators or localized magnetic moments. However, in metallic systems, the presence of conduction electrons introduces a dynamic coupling between the sea of itinerant charges and the localized spins, a relationship that manifests in the Kondo effect.

Jun Kondo's work is an explanation for the anomalous resistivity behavior observed in certain measurements that brings a new spin based approach, helping construct a new way of thinking about the magnetic relationships in metals with magnetic impurities. This section aims to provide a comprehensive overview of the Kondo effect, starting with the classical understanding of resistivity in metals, followed by the experimental observations that challenged this view, and culminating in Kondo's theoretical resolution of the resistivity minimum.

2.2.1 The classical view of resistivity

The electrical resistivity of a conductor is a measure of how strongly it opposes the flow of electric current [25]. In most metallic systems, particularly at temperatures above a few Kelvin, the dominant mechanism for electrical resistance comes from the scattering of conduction electrons by lattice vibrations, known as phonons [9]. As temperature decreases, the amplitude of thermal vibrations of the lattice atoms diminishes, leading to a corresponding reduction in the occurrence of electron-phonon scattering events. In addition to dynamic phonon scattering, electrons also scatter from static imperfections such as impurities and lattice defects. The contribution from these static scatterers, known as the residual resistivity, is largely independent of temperature. Consequently, the total resistivity of a typical metal can be expressed as:

$$\rho(T) = \rho_{ph}(T) + \rho_0, \tag{2.7}$$

where $\rho_{ph}(T)$ is the temperature-dependent resistivity due to phonon scattering and ρ_0 is the residual resistivity due to static imperfections.

This equation predicts a monotonic decrease in resistivity as temperature approaches absolute zero, where phonon scattering vanishes, leaving only the residual

resistivity.

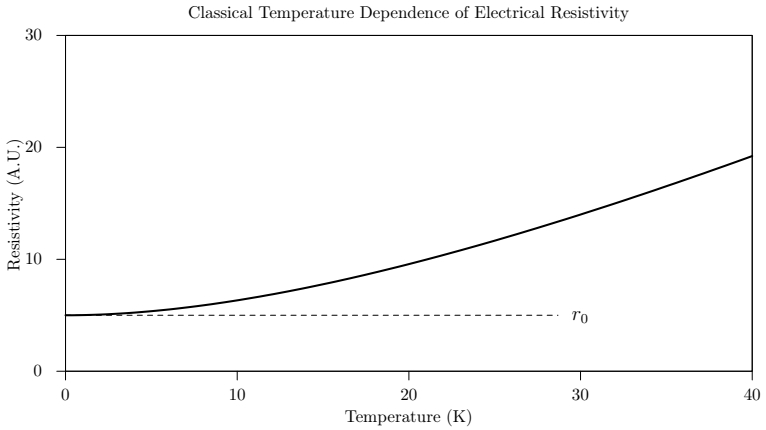

Figure 6 – Schematic illustration of the classical temperature dependence of electrical resistivity in a pure metal. The total resistivity $\rho_{ph}(T)$ decreases monotonically with decreasing temperature, approaching the constant residual resistivity ρ_0 at absolute zero. This behavior reflects the dominant role of electron-phonon scattering, which decreases with temperature, and the temperature-independent scattering from impurities and defects. Source: Author.

Figure 6 illustrates this characteristic monotonic decrease in resistivity with decreasing temperature for a generic metallic system. The total electrical resistivity, $\rho(T)$, is seen to decrease continuously as temperature lowers. At temperatures significantly above the Debye temperature (T_D), a characteristic temperature that reflects the maximum frequency of lattice vibrations in a solid [9], the phonon contribution to resistivity, $\rho_{ph}(T)$, typically exhibits a nearly linear dependence on temperature. This linear regime arises because all phonon modes are thermally excited. Conversely, as temperature falls well below T_D, the thermal excitation of phonons becomes increasingly suppressed, leading to a rapid decrease in the density of available scattering centers. In this low-temperature regime, electron-phonon scattering becomes much less probable, and $\rho_{ph}(T)$ follows a much steeper temperature dependence, often described by a T^5 curve, in accordance with the Bloch-Grüneisen theory [9, 10]. The plateau observed at the lowest temperatures in the graph corresponds to the residual resistivity, ρ_0, which represents the minimum resistance due to temperature-independent scattering from static im-

purities and lattice defects inherent in the material. This visually confirms the classical expectation that a metal's resistivity should monotonically decrease as thermal agitation diminishes, eventually settling at a constant value determined by its imperfections.

2.2.2 The resistivity minimum and the Kondo effect

Despite the classical understanding of metallic resistivity, experimental observations in certain dilute magnetic alloys presented a perplexing anomaly. As early as the 1930s, pioneering cryogenic experiments by scientists such as Walther Meissner and Bernhard Voigt revealed that some nominally pure metals, particularly those containing trace amounts of magnetic impurities (e.g. gold with iron impurities, copper with manganese), exhibited a distinct minimum in their electrical resistivity at low temperatures, typically in the range of a few Kelvin to tens of Kelvin [26]. Further observations confirming this unexpected behavior were made by de Haas, de Boer, and van den Berg (1934), solidifying the experimental evidence for this phenomenon [27]. Below this minimum, instead of continuing to decrease towards a constant residual value, the resistivity began to increase significantly with further cooling. This deviation from classical metallic behavior is graphically illustrated in Figure 7.

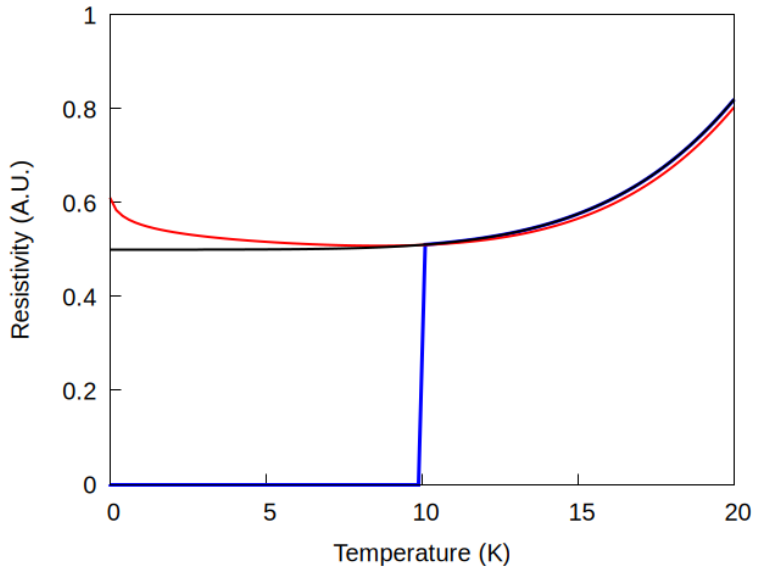

Figure 7 – Comparison of classical and Kondo resistivity behavior. The black line represents the classical expectation of resistivity decreasing with temperature, while the red line illustrates the anomalous upturn in resistivity observed in dilute magnetic alloys at low temperatures, known as the Kondo anomaly and the blue line indicates the superconductivity. Source: Author.

This upturn behavior in resistivity at very low temperatures, commonly referred to as the "resistivity minimum" or the "Kondo anomaly", stood in direct contradiction to the classical expectation of monotonically decreasing resistivity as thermal vibrations subside. Traditional models of electron scattering, including those considering simple potential scattering from isolated impurities, could not account for this puzzling temperature dependence. Such models would predict only a temperature-independent contribution to resistivity from static impurities. The observed increase in resistance as temperature approached absolute zero was therefore a profound challenge to the prevailing theories of electronic transport, giving rise to what became known as the "Kondo problem".

2.2.3 Jun Kondo's resolution of minimum resistivity

The anomalous resistivity minimum posed a challenge to the conventional understanding of electronic transport in metals. This puzzling upturn in resistivity at

very low temperatures, contrary to the expected monotonic decrease, could not be explained by existing theories, which relied on classical approaches or lower-order perturbation treatments of electron scattering. While such theories adequately accounted for temperature-independent impurity scattering and phonon-induced resistance, they consistently failed to capture the re-increasing resistance observed as temperature approached absolute zero. This unresolved "Kondo problem" highlighted a fundamental limitation in the understanding of electron-impurity interactions in the quantum mechanical regime.

The crucial breakthrough came in 1964 with the pioneering theoretical work of Jun Kondo [28]. His investigation focused on the s-d exchange interaction, a fundamental magnetic coupling where localized magnetic moments (often arising from d- or f-electrons of an impurity atom) interact with the spins of the itinerant conduction electrons in the host metal [6]. This interaction is typically antiferromagnetic, since the localized impurity spin prefers to align antiparallel to the spins of the conduction electrons in its vicinity.

Prior to Kondo's work, theoretical attempts to describe this interaction using perturbation theory, particularly at first order in the exchange coupling constant (J), only yielded a temperature-independent scattering contribution to resistivity. However, this simplified approach neglected crucial higher-order processes. As researchers pushed these calculations to higher orders, they encountered a significant theoretical obstacle: the logarithmic divergence. Specifically, early perturbation calculations for the scattering amplitude indicated the emergence of terms that diverged logarithmically as temperature approached zero. This divergence, when considered for the resistivity, would imply a nonphysical infinite scattering rate at T=0 K [6, 28]. This signaled a breakdown of conventional perturbation theory in the low-temperature regime, indicating that the simple electron-impurity scattering picture was insufficient and that a more sophisticated many-body approach was required.

Jun Kondo's proposal lay in meticulously extending the perturbation theory to third order in the exchange coupling J for the electrical resistivity [28]. By carefully including specific higher-order scattering processes, particularly those involving spin-flip scattering of both the conduction electron and the impurity's electron, he demonstrated that the previously encountered logarithmic divergence was not

a mathematical breakdown but, in fact, the key to the anomalous resistivity. He showed that the contribution to the electrical resistivity arising from the scattering of conduction electrons by the localized magnetic impurities could be expressed as:

$$\rho_{mag}(T) = \rho_{imp} + \rho_{Kondo}(T), \tag{2.8}$$

Where ρ_{imp} represents the temperature-independent part (from first-order scattering), and $\rho_{Kondo}(T)$ is the new, temperature-dependent term:

$$\rho_{Kondo}(T) = -J^2\mathcal{N}(0)\ln\left(\frac{k_BT}{D}\right). \tag{2.9}$$

Here, J is the exchange coupling constant, $\mathcal{N}(0)$ is the density of states at the Fermi level, k_B is the Boltzmann constant, and D is an energy cutoff roughly equivalent to the bandwidth or Fermi energy [6, 28].

Crucially, for the antiferromagnetic coupling ($J < 0$) relevant to the Kondo effect, the term J_2 is positive, but the presence of the negative sign before the logarithmic term means that $\rho_{Kondo}(T)$ increases as temperature decreases. When this contribution is added to the conventional phonon resistivity ($\rho_{ph}(T)$, which decreases with temperature) and the residual resistivity (ρ_0), the total resistivity takes the form:

$$\rho(T) = \rho_0 + \rho_{ph}(T) - J^2\mathcal{N}(0)\ln\left(\frac{k_BT}{D}\right). \tag{2.10}$$

This equation explains the experimentally observed resistivity minimum. At higher temperatures, the decreasing phonon contribution dominates, causing the overall resistivity to drop. However, at lower temperatures, the negative logarithmic term from the Kondo interaction becomes increasingly significant, eventually overpowering the diminishing phonon contribution and leading to the characteristic upturn, forming the minimum.

2.2.4 From Single Impurity to Kondo Lattice

The success of the Single Impurity Kondo Problem (SIKP) in explaining the low-temperature resistivity minimum is limited to dilute alloys. In dense systems,

such as the rare-earth and actinide compounds that exhibit heavy fermion behavior, the magnetic ions are arranged periodically, requiring the use of the Kondo Lattice Model (KLM) to capture the collective physics at low temperatures [6].

The periodic nature of the magnetic ions introduces a second, critical energy scale: the Ruderman-Kittel-Kasuya-Yosida (RKKY) exchange interaction [9, 10]. The RKKY interaction is an indirect exchange mechanism mediated by the spin polarization of the conduction electron sea, leading to inter-site magnetic coupling between the localized moments $\mathbf{S}_i$ and $\mathbf{S}_j$. The RKKY interaction typically favors some form of magnetic ordering, most often antiferromagnetism [1].

2.2.5 The Doniach Competition and Phase Diagram

The low-energy ground state of the KLM is dictated by the competition between these two characteristic energy scales:

- **Kondo Screening**: Favors the formation of a local spin singlet state, which binds the localized moment $\mathbf{S}_i$ to the conduction electron spin $\mathbf{s}_i$. The resulting non-magnetic state is the Heavy Fermi Liquid (HFL).
- **RKKY Exchange**: Favors long-range magnetic ordering, competing with the local screening.

This fundamental competition was qualitatively summarized by Doniach in his seminal phase diagram [29], governed by the dimensionlessdw parameter J_K.

Small J_K: The RKKY interaction dominates, leading to a magnetically ordered ground state. Large J_K: The Kondo screening dominates, leading to a non-magnetic HFL ground state.

The transition point between these two regimes is a Quantum Critical Point (QCP). At this QCP, the coherence of the HFL state breaks down, potentially leading to unconventional non-Fermi liquid behavior and phenomena such as Kondo Breakdown [30].

The Doniach phase diagram is schematically illustrated in Figure 8.

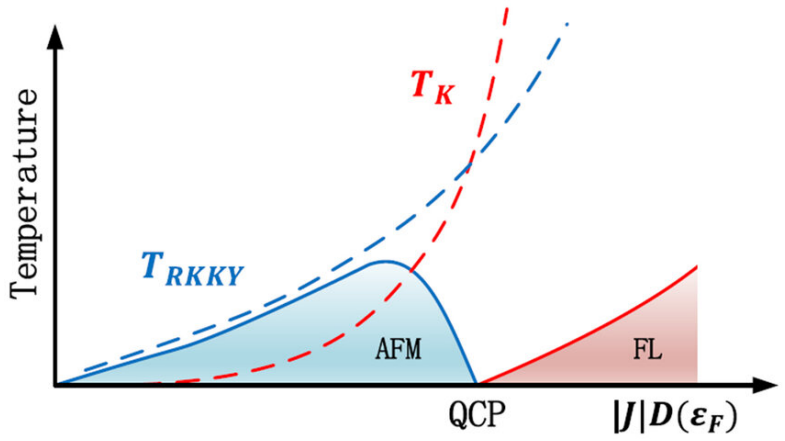

Figure 8 – Schematic Doniach phase diagram illustrating the competition between Kondo screening and RKKY interaction as a function of the Kondo coupling strength J_K. The diagram shows the transition from a magnetically ordered phase at low J_K to a Heavy Fermi Liquid (HFL) phase at high J_K, with a Quantum Critical Point (QCP) marking the boundary between these two regimes. Source: [31]. Source: Author.

2.3 Interplay between magnetic ordering and Kondo interactions

When Kondo screening is present in a magnetic system, it can significantly influence the magnetic ordering and phase transitions. The Kondo effect arises from the interaction between localized magnetic moments and conduction electrons, leading to the formation of Kondo singlets at low temperatures [6]. That occurs when the conduction electrons bind to the localized moments, by forming a singlet state when the conduction electron spin is antiparallel to the localized moment spin. This binding has a lower energy than the unbound state, leading to a screening of the localized moments.

In a frustrated system, either by geometry or competing interactions, the presence of Kondo screening shows interesting effects. The Kondo effect tends to suppress magnetic ordering by screening the localized moments, which can lead to a reduction in the critical temperature for magnetic phase transitions [6]. In frustrated systems, where magnetic ordering is already weakened due to compe-

ting interactions, the addition of Kondo screening can further destabilize ordered phases, potentially leading to novel ground states such as spin liquids or non-Fermi liquid behavior.

An interesting example for this competition is found in the family of pyrochlore iridates: $Pr_2Ir_2O_7$ [32]. This system exhibits geometric frustration arising from the magnetic moments of the Ir ions. It also displays an antiferromagnetic-to-paramagnetic quantum critical point and hosts complex phenomena such as the Kondo effect. The proposed ground-state phase diagram for this system is shown in Figure 9. In particular, increasing frustration, represented by the parameter G, drives the system from a long-range antiferromagnetic ordered to a quantum paramagnetic phase. On the other hand, as the Kondo coupling J_K increases, the single-ion Kondo effect becomes dominant, corresponding to the yellow region labeled P_L. In the regime of simultaneously strong geometric frustration (G) and Kondo hybridization (J_K), the system exhibits enhanced complexity, with the possible emergence of unconventional forms of quantum criticality [32].

Although the family of pyrochlore iridates exhibits very intriguing results, it represents a challenging system to model theoretically. However, an alternative approach is to consider a model in which the degree of frustration and the Kondo hybridization can be simultaneously tuned, ranging from weak to strong frustration and from weak to strong hybridization. A promising model to adjust degree of frustration is given by the $J_1 - J_2$ model, where the ration $J_2/|J_1|$ can turn frustration. The Kondo coupling can also be incorporated, leading to a Kondo–J_1–J_2 model, which belongs to the class of Kondo–Heisenberg models. As a result, the J_1–J_2 model in the presence of Kondo interactions alters the balance between competing magnetic orders and the Kondo effect. This is precisely the model considered in the next chapter.

2.4 Cluster Mean-Field

While standard Single-Site Mean-Field (MFT) Theory provides a qualitative description of phase transitions, it often fails in the presence of strong electronic correlations and geometric frustration. In the $J_1 - J_2$ model, the point of maximum frustration ($J_2/J_1 \approx 0.5$) is characterized by intense short-range correlations that

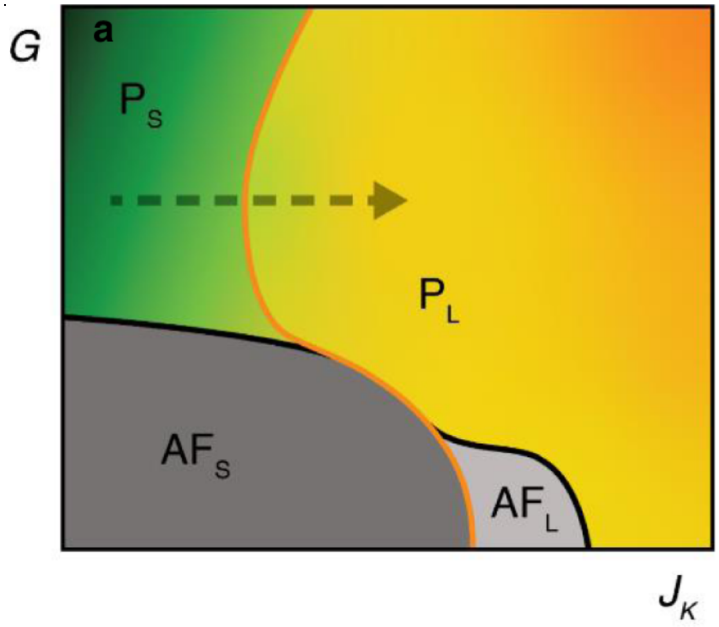

Figure 9 – Schematic phase diagram of the frustrated Kondo lattice in $Pr_2Ir_2O_7$. AF_S represents an antiferromagnetic ordered phase, AF_L denotes the coexistence of antiferromagnetic order of the localized moments with Kondo singlet formation, P_L corresponds to a phase dominated by Kondo singlets, and P_S denotes a quantum paramagnetic phase [32].

single-site approximations neglect, leading to an overestimation of the magnetic transition temperatures and a failure to capture non-magnetic phases [8].

The Cluster Mean-Field (CMF) approach is employed here to mitigate these deficiencies. By treating a small cluster of sites (in this work, $N_c = 4$) exactly via exact diagonalization and only approximating the inter-cluster interactions as an effective field, we preserve the intra-cluster quantum fluctuations and short-range correlations [33]. This method is particularly robust for identifying the change in the nature of phase transitions, such as the first-order transitions often found between the Néel and Collinear phases, which standard MFT frequently mischaracterizes as continuous [34].

Despite its advantages over local MFT, the current implementation carries intrinsic limitations that must be acknowledged:

- **Finite-Size Effects:** The use of a 4-site cluster introduces a discrete symmetry that may artificially stabilize specific magnetic configurations, such as

the SAF phase, compared to the thermodynamic limit.

- **Mean-Field Bias:** While intra-cluster correlations are exact, the method still relies on a broken-symmetry field. This typically leads to the persistence of long-range order at temperatures where, in lower dimensions, Mermin-Wagner fluctuations might suppress it.

- **Kondo Coherence:** The mean-field treatment of the J_K interaction may not fully capture the complex frequency dependence of the self-energy associated with the formation of a fully coherent Heavy Fermion liquid, focusing instead on the competition between the local singlet and the magnetically ordered states.

It is imperative to note that the finite transition temperatures (T_N and T_{SAF}) obtained in this work stand in apparent contrast to the Mermin-Wagner theorem, which forbids the spontaneous breaking of continuous symmetry in two dimensions at $T > 0$. In the CMF framework, the inter-cluster interaction is treated via an effective field that assumes a symmetry-broken state a priori. Consequently, while CMF provides a superior description of the $J_1 - J_2$ competition compared to standard MFT, the resulting phase boundaries should be interpreted as indicating the strength of the underlying correlations rather than a rigorous prediction of a 2D phase transition.

3 Model

To model the physical system under study, a two-dimensional square lattice with localized spins and conduction electrons is used. Since for a lattice with a huge number of sites the Hamiltonian is not exactly solvable, a mean-field approximation is employed to treat the problem. In this approach, the lattice is divided into small clusters, focusing on the exact solution for the interactions inside the clusters. The interactions between clusters are treated using self-consistent mean-field parameters. This chapter describes the Hamiltonian used to model the system and the mean-field approximation technique applied to solve it.

3.1 Hamiltonian

The model adopted in this work is the $J_1 - J_2$ Ising model on a square lattice, with electron hopping (RKKY interaction) and Kondo interactions. The Hamiltonian is given by

$$\mathcal{H} = J_1 \sum_{\langle i,j \rangle} S_i \cdot S_j + J_2 \sum_{\langle\langle i,k \rangle\rangle} S_i \cdot S_k - t \sum_{\langle i,j \rangle,\sigma} (c^\dagger_{i\sigma} c_{j\sigma} + h.c.) + J_K \sum_i \mathbf{S}_i \cdot \mathbf{s}_i, \quad (3.1)$$

where the two first terms represent both the first and second nearest-neighbor Heisenberg interactions, where J_1 and J_2 are the exchange interaction strengths for nearest and next-nearest neighbors, respectively. The notation $\langle i, j \rangle$ indicates a sum over nearest-neighbor pairs, while $\langle\langle i, k \rangle\rangle$ indicates a sum over next-nearest-neighbor pairs. S_i is the Ising spin operator at site i. These terms can be expressed separately as

$$\mathcal{H}_{J1-J2} = J_1 \sum_{\langle i,j \rangle} S_i \cdot S_j + J_2 \sum_{\langle\langle i,k \rangle\rangle} S_i \cdot S_k. \quad (3.2)$$

The next term represents the hopping of the conduction electrons. It is written in terms of the creation $c^\dagger_{i\sigma}$ and annihilation $c_{j\sigma}$ electron operators at sites i and j with spin projection σ. Here, t is the hopping amplitude and $h.c.$ stands for the Hermitian conjugate, as Equation 3.3 shows.

$$\mathcal{H}_{hop} = -t \sum_{\langle i,j \rangle, \sigma} (c^{\dagger}_{i\sigma} c_{j\sigma} + h.c.). \tag{3.3}$$

The term H_{hop} in Equation 3.3 is the kinetic hopping term of the conduction electrons, mediated by the parameter t. This term describes the movement of electrons between lattice sites, while the RKKY interaction is an effective, indirect, long-range exchange interaction between the localized magnetic moments (S_i) that arises from the combined effect of the kinetic term (H_{hop}) and the on-site Kondo coupling (H_{Kondo}) [1, 9]. The conduction electrons are polarized by the localized moments via H_{Kondo}, and this polarization propagates through the lattice via H_{hop}, leading to an oscillatory, distance-dependent exchange coupling between the localized spins. Since the Hamiltonian already includes explicit J_1 and J_2 spin-spin couplings, the H_{hop} term is formally described as the kinetic energy, acting as the mediator for the magnetic correlation.

At last, the Kondo interaction term describes the coupling between the localized spins $\mathbf{S}_i$ and the spin of the conduction electrons $\mathbf{s}_i$ at site i. The Kondo coupling constant is denoted by J_K, as shown in Equation 3.4.

$$\mathcal{H}_{Kondo} = J_K \sum_i \mathbf{S}_i \cdot \mathbf{s}_i. \tag{3.4}$$

Here the $\mathbf{S}_i$ denotes the localized spin operator at site i, and $\mathbf{s}_i$ represents the spin operator of the conduction electrons at the same site. The **bold** notation indicates that these are Heisenberg spin operators, which have components in all three spatial directions (x, y, z).

A critical decision in the Cluster Mean-Field (CMF) formulation is the treatment of the electron kinetic energy. In this work, the hopping term (t) is strictly limited to sites within the 4-site cluster, while the inter-cluster hopping (t_{inter}) is set to zero. This choice was taken to enforce a canonical ensemble for the cluster's electron number. If inter-cluster hopping were permitted, it would also require a mean-field decoupling, effectively connecting the cluster to an external 'electron bath' and treating it as a grand-canonical system. In such a scenario, the electron number (n_c) would fluctuate around a non-integer average ($\langle n_c \rangle$), introducing numerical instabilities and discontinuities in observables. By setting $t_{\text{inter}} = 0$, the system is defined as a lattice of 4-site clusters that are electronically isolated but

magnetically coupled (via the J_1 and J_2 mean-field terms). This allows for controlled investigation of the local physics as a direct function of a fixed, integer electron filling ($n_c \in \{0, 1, 2, 3, 4\}$).

The primary cost of this simplification is the neglect of phenomena driven by long-range electronic coherence. Specifically, the absence of t_{inter} prevents the formation of a coherent, large Fermi surface characteristic of the true metallic state in the full Kondo lattice model. Consequently, the calculation cannot capture effects associated with long-range charge transport (e.g., electrical conductivity) or charge-based instabilities across the lattice. However, for the central goal of isolate and quantify the competition between magnetic frustration and the local formation of the Kondo singlet, the canonical CMF treatment provides a powerful framework.

3.2 Cluster Mean-Field Approximation

As the general Hamiltonian is not exactly solvable, a technique called mean-field approximating was employed. In this approach, decoupling the interactions is done by introducing mean-field parameters that represent the average behavior of the system. This approximation allows us to reduce the many-body problem into a more manageable form by splitting the lattice structure into clusters, as shown in Figure 10. By doing so, the interactions within each cluster can be treated exactly, while the interactions between clusters are approximated using mean-field parameters.

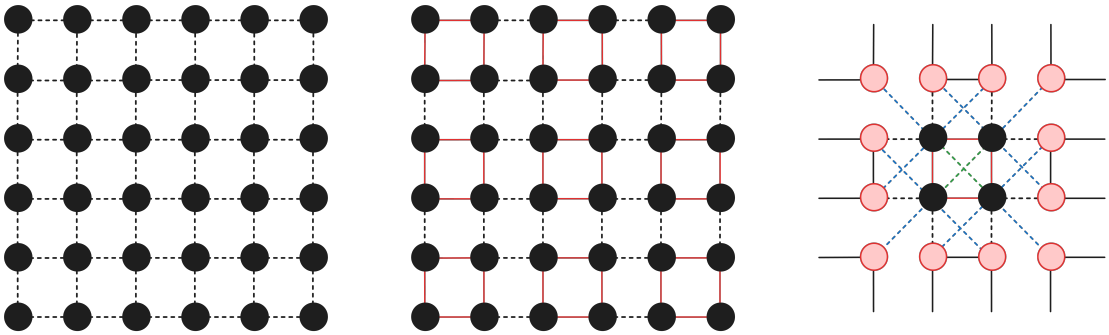

Figure 10 – Full lattice structure on the left, cluster represented on center and interactions on the right. Intra-cluster interactions in solid lines, inter-cluster interactions in dashed lines. Red and Black represents first nearest neighbors, blue and green represents second-nearest neighbors.

3.2.1 Intra-cluster Interactions

To solve intra-cluster interactions exactly diagonalization techniques was used. This involves constructing the Hamiltonian matrix for each cluster, following Equation 3.1 for 4 sites and n electrons, [1] and finding its eigenvalues and eigenvectors using Equation 3.5.

$$\mathcal{H}_{cluster} = UDU^{\dagger}, \tag{3.5}$$

where D is the Hamiltonian in non-diagonal form, and U is the eigenvector matrix.

3.2.2 Inter-cluster Interactions

Using the previous results, the inter-cluster interactions are treated using mean-field parameters. This involves replacing the operators in the Hamiltonian with their average values, effectively reducing the complexity of the problem. When replacing the operators in the Hamiltonian, the interactions between sites of the same cluster are treated with an intra-cluster interaction exactly as shown in Equation 3.2 and between different clusters' sites are treated as seen the thermodynamic

[1] n should be smaller or equal than twice the site spins, in this case $n \leq 8$, since the net spin of 2 electrons on the same site is zero, due to Pauli Exclusion Principle, it's possible to consider equal to the number of sites, $n \leq 4$ in this case.

average of the corresponding intra-cluster site magnetization, as shown in Equation 3.6.

$$\begin{aligned}\mathcal{H}^{MF}_{J1-J2} = J_1 \left(\sum_i^4 S_i \cdot S_{i+1} + \sum_i^4 \left(S_i \cdot \langle S_{i-1} \rangle + S_i \cdot \langle S_{i+1} \rangle \right) \right) \\ + J_2 \left(\sum_i^2 S_i \cdot S_{i+2} + 3 \sum_i^4 S_i \cdot \langle S_{i+2} \rangle \right),\end{aligned} \tag{3.6}$$

where

$$\langle S_i \rangle = \frac{Tr(S_i e^{-\beta \mathcal{H}})}{Tr(e^{-\beta \mathcal{H}})}, \tag{3.7}$$

and $\mathcal{H}$ represents the clustered Hamiltonian.

To calculate the interactions using the mean-field approximation, the product of two spin operators is approximated by the sum of the product of one operator and the average value of the other operator, as shown in Equation 3.8.

$$S_i \cdot S_j \approx S_i \cdot \langle S_j \rangle + \langle S_i \rangle \cdot S_j - \langle S_i \rangle \cdot \langle S_j \rangle \tag{3.8}$$

$$\mathcal{H} = \mathcal{H}^{MF}_{J1-J2} + \mathcal{H}_{hop} + \mathcal{H}_{Kondo}. \tag{3.9}$$

So $\langle S_i \rangle$ is the Mean Field value of site i, calculated using the thermodynamic average over spin operator on site i by adding the Hamiltonian $\mathcal{H}$ at temperature T (with $\beta = 1/k_B T$, where k_B is the Boltzmann constant).

This is a self-consistent process, where the mean-field parameters are updated iteratively until convergence is achieved. The final mean-field Hamiltonian captures the magnetic properties of the system, allowing for the study of phase transitions and magnetic ordering.

3.2.3 Observable Calculation

With the Hamiltonian calculated, various observables can be computed to analyze the system's behavior. Key observables include the local magnetization, spin-spin correlation functions, and Kondo singlet formation indicators.

The general expression for calculating the thermodynamic average of an operator $\mathcal{O}$ is given by

$$\langle \mathcal{O} \rangle = \frac{Tr(\mathcal{O} e^{-\beta \mathcal{H}})}{Z}, \tag{3.10}$$

just like the mean-field parameters in Equation 3.7.

Specifically, the partition function Z, which is crucial for calculating thermodynamic properties is computed as

$$Z = Tr(e^{-\beta\mathcal{H}}). \tag{3.11}$$

Using the partition function, the free energy F of the system can be determined:

$$\mathcal{F} = -k_B T \ln(Z) + J_1(m_1 + m_3)(m_2 + m_4) + 3J_2(m_1 m_3 + m_2 m_4). \tag{3.12}$$

Here, $m_i = \langle S_i \rangle$ represents the mean-field magnetization at site i.

The correlation functions between localized spins and between localized spins and conduction electron spins are also calculated. The spin-spin correlation function between localized spins at sites i and j is given by

$$\langle S_i \cdot S_j \rangle = \frac{Tr(S_i \cdot S_j e^{-\beta\mathcal{H}})}{Z}, \tag{3.13}$$

The second correlation function computes the interaction between second-nearest neighbors, given by

$$\langle S_i \cdot S_k \rangle = \frac{Tr(S_i \cdot S_k e^{-\beta\mathcal{H}})}{Z}, \tag{3.14}$$

where k is the second-nearest neighbor of site i.

Finally, the correlation function between localized spins and conduction electron spins at the same site is calculated as

$$\langle \mathbf{S}_i \cdot \mathbf{s}_i \rangle = \frac{Tr(\mathbf{S}_i \cdot \mathbf{s}_i e^{-\beta\mathcal{H}})}{Z}. \tag{3.15}$$

These observables provide insights into the magnetic ordering, Kondo singlet formation, and overall behavior of the system under various conditions, such as temperature, exchange interactions, and Kondo coupling strength.

4 Numerical Procedures

The Numerical procedures on this work was implemented in Fortran [35]. Fortran was chosen due to its efficiency in handling large numerical computations and matrix operations, which are essential for the diagonalization of the Hamiltonian matrix and the iterative cluster mean field calculations required in this study. The language's robust support for array manipulations and mathematical functions makes it well-suited for the complex calculations involved in modeling the J_1-J_2 Kondo lattice system.

A full, multistage algorithm was developed to solve the Hamiltonian in Equation 3.1, those stages are represented in Figure 11.

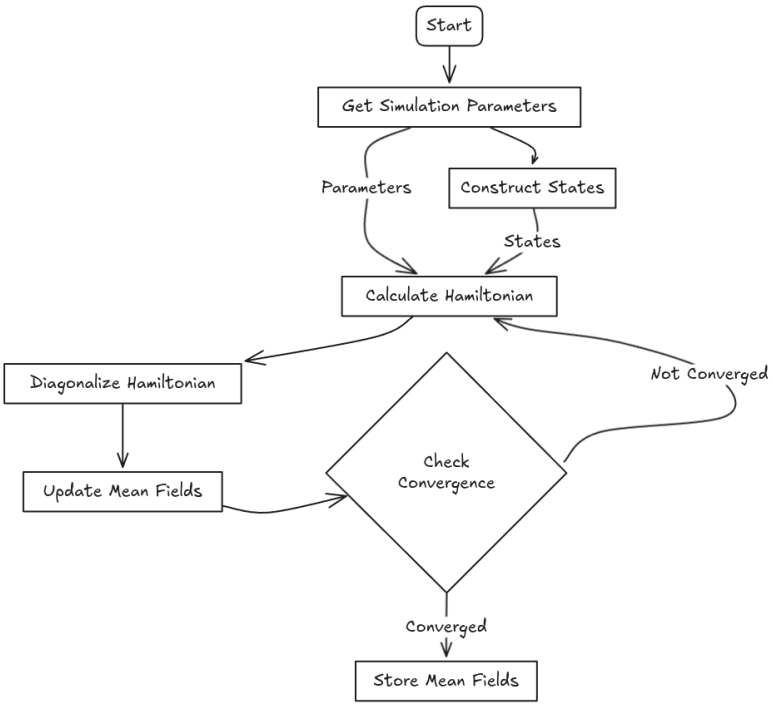

Figure 11 – Schematic representation of the code structure, illustrating the main components and their relations. Source: Author.

The code starts by getting the simulations parameters (i.e. Number of electrons, J2, JK, Temperature, Initial Mean Fields) from an input file, with the

number of electrons the states are constructed. To calculate the Hamiltonian matrix, the initial cluster mean field values are considered. The Hamiltonian gets diagonalized and the cluster mean fields are calculated. The Hamiltonian gets calculated and diagonalized once more and the cluster mean fields are compared with its previous value, if they are within a tolerace the cycle stops and the cluster mean fields value for each site are stored.

4.1 States creation and Properties

The goal was to achieve a solution for representing first the site state of the system, such partial state is the representation of a 4 site square lattice, with no conduction electrons.

First, all the possible configurations of the spins of the cluster can be written as a binary representation, where each bit represents the state of a spin (up or down). This representation consists of storing each of the site configurations in an integer variable, so some performance could be gained. To facilitate the understanding of the algorithm a few examples could illustrate the point. The following examples will introduce the notation used to represent the states both as integer and ket notation, as:

- All spins down: $|0\rangle = 0000$
- First spin up, others down: $|1\rangle = 0001$
- First and last spins up, others down: $|9\rangle = 1001$
- All spins up: $|15\rangle = 1111$

In this representation, the integer inside the bracket is expressed as a bit sequence on the right side of the expression. The position of a particular bit corresponds to the site where the spin is noted. For instance, the notation $|9\rangle = 1001$ represents a spin configuration in which the first site can be occupied by spins up (bit set as "1"), while the two central bits, set as "0", correspond to spins down. Figure 12 illustrates the arrangement of these spin states of four-site clusters on a

square cell, showing from left to right the states represented by $|0\rangle$, $|1\rangle$, $|9\rangle$, and $|15\rangle$, respectively.

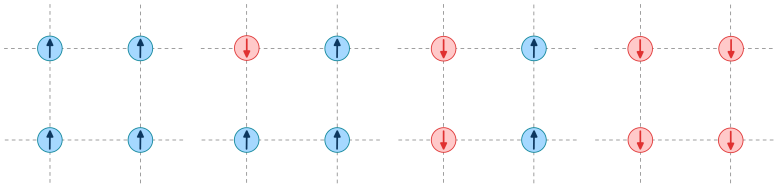

Figure 12 – The counting of sites is done starting from the top left site and going clockwise, finishing in the forth site on the bottom left. On the left of the frame is the $|0\rangle$ state, on the center left is the $|1\rangle$ state, followed by $|9\rangle$ on the center right and on the right of the frame is $|15\rangle$. Source: Author.

With all site states defined for a finite cluster, the Ising Hamiltonian matrix can be constructed by checking the alignment of neighboring spins for each state, for first neighbors the state $\|0\rangle$ has all spins down, so all neighboring pairs are aligned, resulting in a contribution of 1 for each pair, leading to a total contribution of 4 to the diagonal on $|0\rangle$ x $|0\rangle$. The state $|1\rangle$ has one spin up and three spins down, resulting in two neighboring pairs aligned and two pairs anti-aligned, leading to a contribution of 0 to the diagonal on $|1\rangle$ x $|1\rangle$, and so on. The same procedure is repeated for second neighbors, resulting in another matrix. Both matrices are then multiplied by their respective J1 and J2 parameters and summed to obtain the Ising interaction matrix.

For the Heisenberg interaction, the quantum term is added to a matrix on the corresponding off diagonal terms. The way this is done is by iterating over all states and checking if flipping a pair of neighboring spins results in another valid state, if it does, the contribution is 1/2 on $|n\rangle \times |n'\rangle$, where $|n'\rangle$ is the state with the flipped spins. This procedure is repeated for all first and second neighbors, resulting in the Heisenberg interaction matrix, which is then multiplied by the J1 and J2 parameters and summed to the Ising interaction matrix to obtain the full Heisenberg interaction matrix.

Now that the site states are defined, the next step is to introduce the hopping term, which is represented in terms of conduction electron states. The electrons are expressed in second quantization by creation and annihilation operators. There-

fore, the numerical formalism should be adequate for this purpose. The conduction electrons are represented by a pair of bits for each site, so for each possibility of occupation of the site are accounted for. The logic is to represent all binary masks of electrons with spin up on the first 4 bits of the integer, the binary masks of spins down on the next 4 bits and lastly the site states, also 4 bits. This way a few performance points can be leveraged by using bitwise operations to manipulate the states. It is important to note that the integer representation from this point on is not continuous and the order of the numbers has no relation to the parameters of the system, its only purpose is to represent the states in a compact way. The following examples illustrate the point:

- No conduction electrons, all spins down: $|0\rangle = 0000\ 0000\ 0000$
- One spin down electron on site 1, all spins down: $|16\rangle = 0000\ 0001\ 0000$
- One spin up electron on site 1, all spins down: $|256\rangle = 0001\ 0000\ 0000$
- One spin up electron on site 1 and one spin down electron on site 2, all spins down: $|537\rangle = 0010\ 0001\ 1001$

For the conduction electrons there are 2 interactions at play, the first is electron hopping, which is represented by Equation 3.3. The way this interaction is calculated is by iterating over all the states and checking which state represent the same site state but with an electron hopped to a neighboring site. For example, the state $|16\rangle$ can hop the electron to site 2, resulting in the state $|32\rangle$ (one spin down electron on site 2, all spins down). This is done for all states with first and second neighbors, by constructing a matrix with 1 when the hopping is possible between states and 0 when it is not, and the term is off the main diagonal, on $|m\rangle \times |n\rangle$. For example, the term on $|16\rangle \times |32\rangle$ is 1, since the electron can hop from site 1 to site 2, likewise the term $|16\rangle \times |64\rangle$ is 1 as the electron can hop to the second neighbor. The resulting matrix should be symetric, and it is multiplied by the hopping parameter t and summed to the Hamiltonian matrix.

For the Kondo interaction, represented by Equation 3.4, the way to calculate it is by iterating over all the states and checking if there is a conduction electron on the same site as a localized spin. If there is, the interaction is calculated by checking

if the spins are aligned or anti-aligned. If they are aligned, the contribution is 1/4, if they are anti-aligned, the contribution is -1/4, this procedure provides the diagonal (Ising) terms to the Kondo interaction. To calculate the off diagonal (Heisenberg) terms, the algorithm checks if the state with both site and conduction spin flipped is possible, if it does, the contribution is 1/2 on $|n\rangle \times |n'\rangle$. For example, the state $|16\rangle$ can have a electron flip as well as a site flip on site 1, leading to a contribution of 1/2 on both $|1\rangle \times |16\rangle$ and $|16\rangle \times |1\rangle$. This procedure is repeated for all sites and all states, resulting in the Kondo interaction matrix, which is then multiplied by the Kondo parameter J_K and summed to the Hamiltonian matrix. This completes the construction of the Hamiltonian matrix (Equation 3.1).

4.2 Cluster Mean Field Approximation

The previous Hamiltonian matrix construction is only valid for the intra-cluster interactions, to account for the inter-cluster interactions a cluster mean field approximation is used. The way this is done is by introducing cluster mean field parameters that represent the average behavior of the system.

By diagonalizing the Hamiltonian matrix, a few mathematical entities emerges, an important one is the eigenvector matrix U that after multiplying by the spin matrix S_i the cluster mean field of site i is obtained. The spin matrix is simply a square matrix of size number of states, with the value of the spin at site i on the main diagonal and 0 elsewhere. The cluster mean field is calculated by Equation 3.6. For example, the cluster mean field of site 1 is calculated by diagonalizing the spin matrix of site 1, the resulting matrix is then multiplied by the Boltzmann factor $e^{-\beta \mathcal{H}_{ii}}$ and summed over all states. The result is then divided by the partition function Z, which is the sum of the Boltzmann factors over all states.

Now the trickiest part of the cluster mean field approach is its self-cosnsistency, which means that the cluster mean field parameters are calculated from the Hamiltonian and, oddly enough, the Hamiltonian is constructed using the cluster mean field parameters. To solve this conundrum, an iterative approach is used, where the cluster mean field parameters are initialized with some values, the Hamiltonian is constructed and diagonalized, the cluster mean field parameters are then calculated from the eigenvector matrix and the process is repeated until convergence is

achieved. The initial values are determined by the expected phase of the system on its critical points, a few examples are:

- For a Temperature of $0K$ and a J_2 of 0, the expected phase is antiferromagnetic, so the cluster mean field parameters are initialized with a staggered magnetization of 0.5 and -0.5.
- For a Temperature of $0K$ and a $J_2 \approx J_1$, the expected phase is stripes, so the cluster mean field are with a $(0.5, 0.5, -0.5, -0.5)$.
- For a Temperature of $T \approx J_1$ the expected phase is paramagnetic, so the cluster mean field parameters are initialized with 0.

With those critical points, either the temperature increases a small step or the J_2 parameter increases a small step, and the cluster mean field parameters are initialized with the converged values of the previous step. This way, the system is expected to be close to the new phase, and convergence is achieved faster.

The way the cluster mean fields affect the system is by substituting the spins from outside the cluster with the value obtained by Equation 3.6. A visual representation of the complete system is shown in Figure 13.

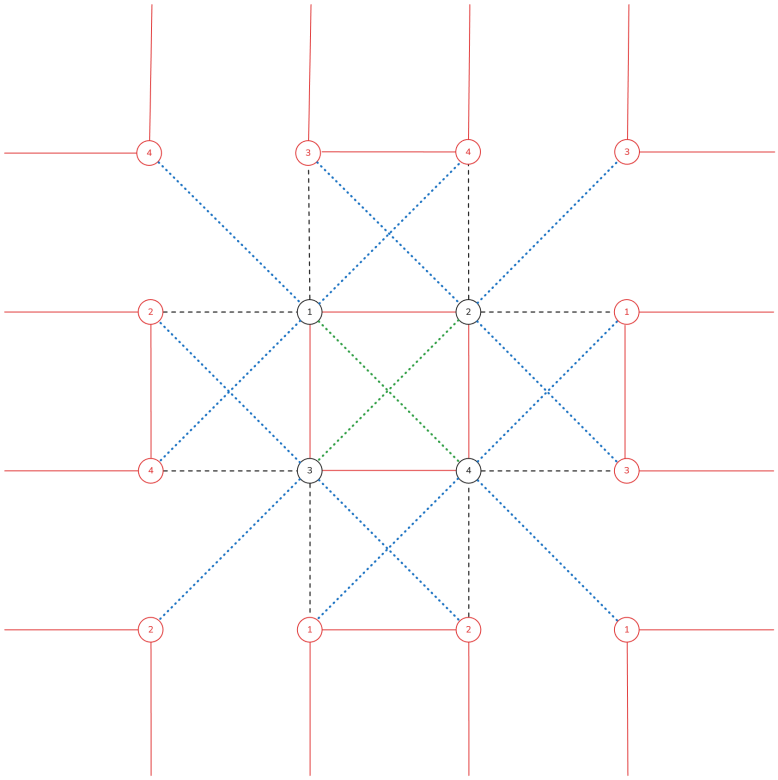

Figure 13 – Red lines represent first nearest neighbors, green lines represent second nearest neighbors, both for intra-cluster interactions. Black lines represent first nearest neighbors, blue lines represent second nearest neighbors, both for inter-cluster interactions. Outside the cluster, all spin values are obtained by the cluster mean field parameters. The numbers represent the cluster mean field values corresponding with the clusters site. Source: Author.

Note that for spins in the cluster the preserved values are those from the intra-cluster interactions (2 first neighbors and 1 second neighbor) and those from the inter-cluster interactions (2 first neighbors and 3 second neighbors with the same cluster mean field value). For example, for spin 1, the intra-cluster interactions are with spins 2 and 3 (first neighbors) and spin 4 (second neighbor), while the inter-cluster interactions are with two cluster mean field values for spins 2 and 3 with first neighbor interaction and three cluster mean field values for spin 4 with second neighbor interaction.

To achieve convergence, the cluster mean field parameters are updated by a

weighted average of the previous value and the new value obtained from Equation 3.6, this is done to avoid oscillations and ensure coherence. The weight is determined by the parameter α, which is set to 0.5 for this work.

To summarize, the cluster mean field parameters as well as the Hamiltonian matrix are updated iteratively by following a few steps:

1. Construct Hamiltonian matrix without mean field.
2. Diagonalize Hamiltonian matrix to obtain eigenvector matrix.
3. Initialize cluster mean field parameters with expected phase values, on critical points.
4. Calculate the complete Hamiltonian matrix (including mean field parameters).
5. Calculate new mean field parameters using Equation 3.6.
6. Update mean field parameters by weighted average with parameter α.
7. Check for convergence, if not converged, repeat from step 4.

Those same steps can be seen in Fig. 11.

For a non-critical point, the convergence is achieved by initializing the cluster mean field parameters with the converged values from the previous step recursively until a critical point, either in temperature or J_2 parameter. The sweeping procedure can be done on both directions, either increasing temperature or J_2 parameter first. This is relevant when dealing with first-order phase transitions, where hysteresis can occur, by fixing the Temperature and sweeping the J_2 parameter, it can be diminished.

4.3 Solving the Hamiltonian

To start solving the Hamiltonian, it's necessary to contruct a few matrices of interactions. Those matrices are constructed by using the interactions. For example, the J_1 matrix is constructed by checking the alignment of the neighboring

spins for each state, therefore this matrix will have contributions only on the main diagonal (Figure 14 A). The same procedure is repeated for the J_2 matrix. Both matrices are then multiplied by their respective parameters and summed to obtain the Ising interaction matrix.

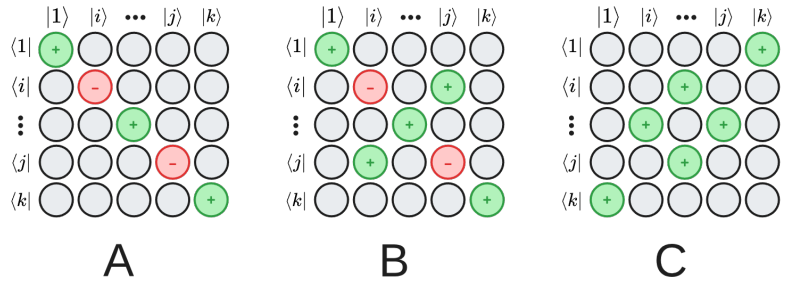

Figure 14 – Schematic representation of the Hamiltonian matrix structure, illustrating the different interaction components and their placements within the matrix, as well as their signs. Source: Author.

Then the hopping matrix is constructed by checking the states with the same lattice arrangement, but with an electron hopped to a neighboring site. This is done for all states with first and second neighbors, resulting in the hopping matrix, which is then multiplied by the hopping parameter t and summed to the Hamiltonian matrix (Figure 14 B). Notice that the hopping term contributes only to the off-diagonal terms of the Hamiltonian matrix.

Finally, the Kondo interaction matrix is constructed by checking if there is a conduction electron on the same site as a localized spin. If there is, the interaction is calculated by checking if the spins are aligned or anti-aligned, leading to contributions on both diagonal and off-diagonal terms (Figure 14 C). This procedure is repeated for all sites and all states, resulting in the Kondo interaction matrix, which is then multiplied by the Kondo parameter J_K and summed to the Hamiltonian matrix.

4.4 Observable Calculation

To acquire the observable of the system, once convergence is achieved, a few calculations are performed using the eigenvector matrix and the Boltzmann factors.

The correlation between sites are calculated by iterating over each state, calculating the product of the spins at the desired sites, multiplying by the Boltzmann factor and summing over all states. The result is then divided by the partition function Z to obtain the correlation value. This procedure repeats for all combinations if first or second neighbors as well as for Z correlation and XY correlation.

Another correlation to calculate is the Kondo correlation, which is calculated by iterating over each state, calculating the thermodynamic average of the product of the localized spin and the conduction electron spin at the same site. The correlation matrix is constructed by placing the product of the site and free electron on the main diagonal, if the state with the opposite spins is possible, the off diagonal term is set to 1/2.

The Helmholtz free energy is calculated by taking the negative logarithm of the partition function Z multiplied by the temperature T, then corrected for the cluster mean field approximation by adding the interaction energy between the cluster mean field parameters and the spins of the cluster for both first and second neighbors. The minimal eigenvalue is also added for the correction.

The results are exported to a text file for further analysis and visualization. The output includes the cluster mean field values, correlation values and Helmholtz free energy for each set of simulation parameters. Tan the software gnuplot [36] is used to visualize the results, by plotting the cluster mean field values and correlation values as a function of temperature and J_2 parameter, phase diagrams are constructed to illustrate the different phases of the system.

To characterize the magnetic phases emerging from the competition between J_1, J_2, and J_K, we define the staggered magnetization for the Antiferromagnetic (AF) and Stripe Antiferromagnetic (SAF) orders. Given the cluster geometry, these order parameters are calculated as the thermal expectation values of the local spin operators at each site i of the cluster:

$$m_{AF} = \frac{1}{4}\left(\langle S_1^z\rangle - \langle S_2^z\rangle + \langle S_3^z\rangle - \langle S_4^z\rangle\right) \tag{4.1}$$

$$m_{SAF} = \frac{1}{4}\left(\langle S_1^z\rangle + \langle S_2^z\rangle - \langle S_3^z\rangle - \langle S_4^z\rangle\right) \tag{4.2}$$

5 Results and Discussions

In this chapter, we discuss the numerical results obtained for the model under consideration. First, the results for the J_1–J_2 model in the absence of Kondo interactions are presented. Subsequently, Kondo interactions are introduced and analyzed for different itinerant electron densities.

5.1 Results for the J_1-J_2 model without Kondo interaction

The approach used in this work was initially validated by comparing the results obtained for the $J_1 - J_2$ model without conduction electrons to those found in the literature. This comparison is carried out using the well-established phase diagram of the J_1–J_2 Ising model [37,38]. In the following, it is discussed how this phase is obtained within the present approach.

The construction of the phase diagram is based on the calculation of the mean field values for various temperatures and $J_2/|J_1|$ ratios. For instance, Figure 15 shows the temperature dependence of the mean fields for different values of $J_2/|J_1|$.

By analyzing the behavior of these mean fields, the critical temperatures for phase transitions were identified. The Néel temperature (T_N) was determined by observing the temperature at which the antiferromagnetic order parameter (m_{AF}) vanishes.

The antiferromagnetic order parameter is defined as $m_{AF} = |(m_1+m_3)-(m_2+m_4)|/4$, indicating that the antiferromagnetic phase corresponds to $m_1 = m_3 = -m_2 = -m_4 \neq 0$, with spontaneous magnetizations alternating between nearest-neighbor sites (sublattices). At higher temperatures, $m_{AF} = 0$, and the system enters the paramagnetic (PM) phase. This discussion is described by Figure 15(A).

Similarly, the critical temperature for the collinear antiferromagnetic phase (T_{SAF}) was found by tracking the disappearance of the corresponding order parameter (m_{SAF}). In this case, the order parameter is defined as $m_{SAF} = |(m_1+m_4)-(m_2+m_3)|/4$ (or equivalently $m_{SAF} = |(m_1+m_2)-(m_3+m_4)|/4$), characterizing a striped antiferromagnetic phase with spontaneous magnetizations alternating

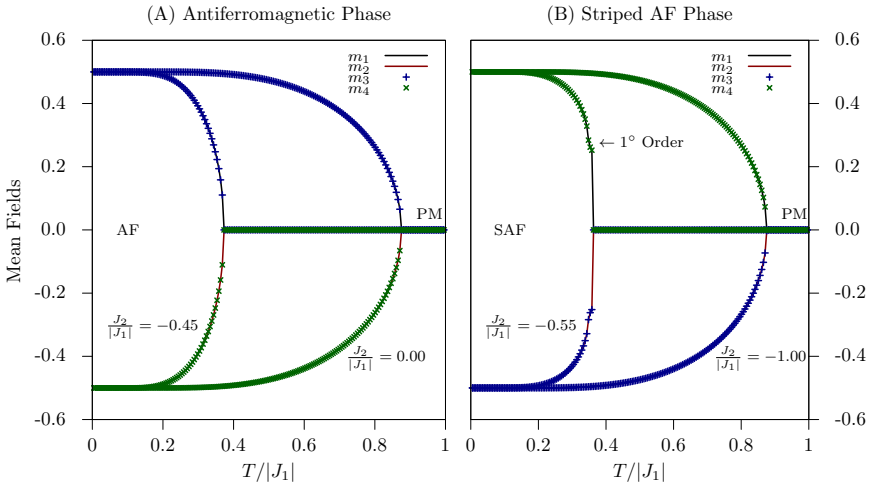

Figure 15 – Mean field magnetizations (order parameters) as a function of temperature for different values of $J_2/|J_1|$. The left panel shows the antiferromagnetic order (order parameter $m_{AF} > 0$), while the right panel displays the collinear antiferromagnetic order ($m_{SAF} > 0$).

between nearest-neighbor columns (or rows) of sites[1].

However, there is a possibility of first-order phase transitions from the SAF order to the PM phase. These transitions are identified by a discontinuous jump in the order parameter, as pointed out in Figure 15-(B). In these cases, the order parameters cannot be used directly to locate the phase transitions. First-order transitions are determined by adopting a free-energy criterion, in which the crossing of different free-energy branches provides an appropriate way to identify the thermodynamically stable phase.

For instance, the m_{SAF} order parameter can exhibit a discontinuous jump, as seen in the right panel of Figure 15 for $J_2/|J_1| = -0.55$. This behavior contrasts with the continuous vanishing of the order parameter observed in second-order transitions, such as those for $J_2/|J_1| = -1.00$ or for $J_2/|J_1| = -0.45$ and 0.00, as shown in the left panel.

The other way to differentiate between first- and second-order transitions in this study was by analyzing the free energy curves of the competing phases. A first-order transition is characterized by a crossing of free energy curves, indicating

[1] Note that $m_{SAF} \neq 0$ corresponds to $m_{AF} = 0$, and vice versa.

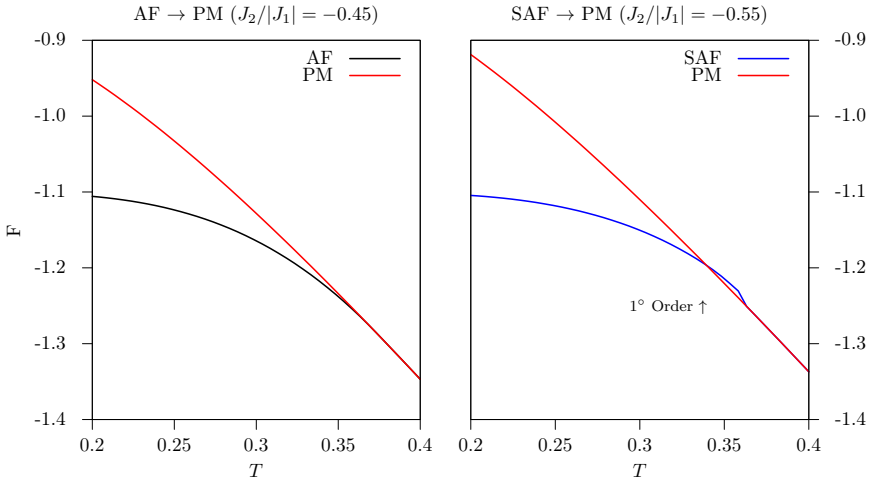

Figure 16 – Free energy as a function of temperature for $J_2/|J_1| = -0.45$ (left) and -0.55 (right). The left panel illustrates a second-order transition from AF to PM. The right panel shows a first-order transition from SAF to PM.

a sudden change in the stable phase. In contrast, a second-order transition shows a smooth convergence of free energy curves without any crossing, reflecting a gradual change in the order parameter. Figure 16 shows typical free-energy behaviors associated with second-order (left panel) and first-order (right panel) phase transitions, where the stable phase corresponds to the minimum free-energy value. The first-order phase transition occurs at the point where the two free-energy curves cross, as indicated by the arrow in the right panel of Fig. 16. On the other hand, a second-order phase transition is characterized by a smooth crossing between the free energies of the two involved orders, as exhibited in the left panel of Fig. 16.

When constructing the phase diagram, Figure 17, the results were first analyzed to establish a baseline for comparison. The dotted lines in the figure represent the phase boundaries obtained from first-order phase transitions, while the solid lines correspond to second-order transitions.

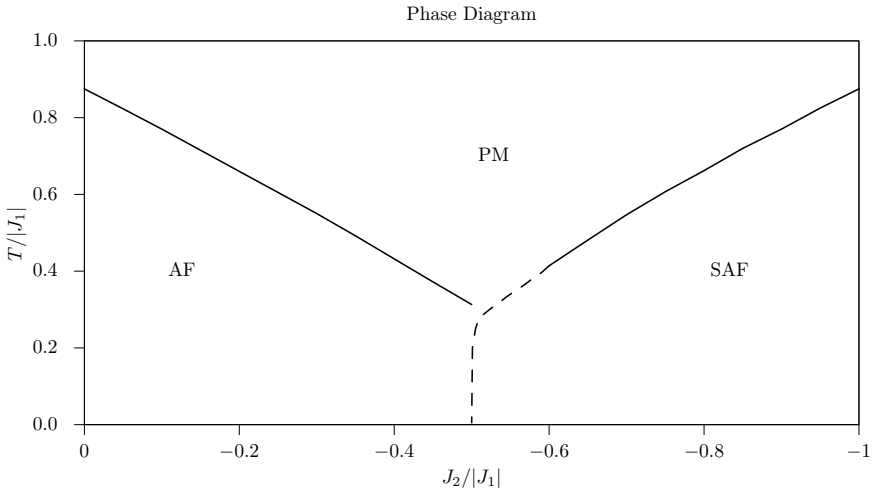

Figure 17 – Phase diagram of the $J_1 - J_2$ model without Kondo interaction, showing the different magnetic phases and their transitions. Solid lines indicate second-order transitions, while dashed lines represent first-order transitions.

The phase diagram of the $J_1 - J_2$ model on a square lattice exhibits three distinct magnetic phases: paramagnetic (PM), antiferromagnetic (AF), and collinear antiferromagnetic (SAF). The transitions between these phases are influenced by the ratio of the exchange interactions $J_2/|J_1|$ and temperature. When the intensity of $J_2/|J_1|$ is small, the system favors the AF phase, while larger values of this ratio lead to the SAF phase. The PM phase dominates at higher temperatures, where thermal fluctuations disrupt magnetic order. However, the transition between the AF and SAF phases occurs around the critical value of $J_2/|J_1| \approx -0.5$, indicating a region of strong frustration where neither phase is energetically favored. The behavior of the transition line from AF to PM phase shows a monotonic decrease in critical temperature as $J_2/|J_1|$ approaches -0.5, staying within the second-order transition regime throughout all the PM/AF phase boundary. The SAF to PM transition line, on the other hand, exhibits a more complex behavior. It starts as a second-order transition at higher temperatures but becomes a first-order transition as it approaches the higher frustration levels from $J_2/|J_1| \lesssim -0.5$ This change in the nature of the transition reflects the increased competition between magnetic orders in this frustrated region. It is important to remark that the phase diagram obtained in Fig. 17 recovers the results for the cluster mean-field method presented

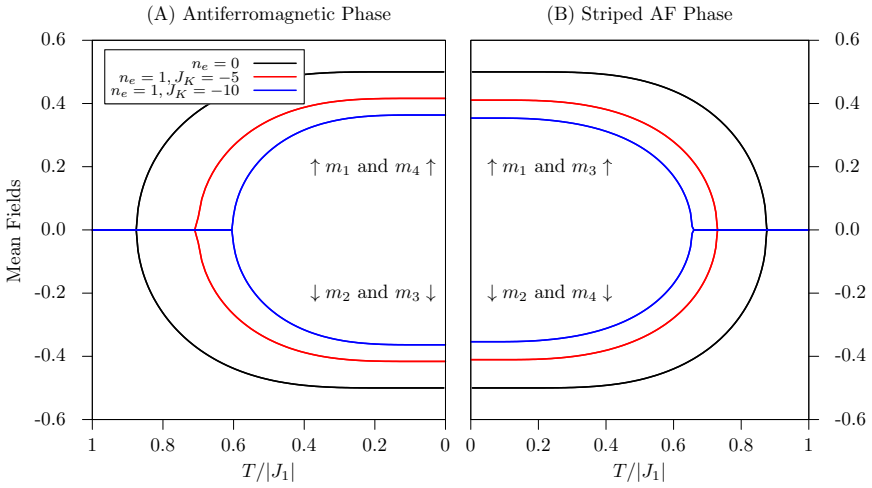

Figure 18 – Mean field parameters as a function of temperature for different values of Kondo interaction $J_K/|J_1|$ at low conduction electron density ($n = 1$ and 0). The left panel shows the antiferromagnetic order parameter m_{AF}, while the right panel displays the collinear antiferromagnetic order parameter m_{SAF}.

in reference [37] for a four-site cluster.

5.2 Results for the J_1-J_2 model with Kondo interaction

The inclusion of Kondo interactions introduces additional complexity to the magnetic behavior of the system. There are two different regimes to be analyzed, one for high density of conduction electrons ($n = 4$) and another for low density ($n = 1$). The main difference between these two regimes lies in the availability of conduction electrons to screen the localized magnetic moments through the Kondo effect, leading to distinct phase transitions.

5.2.1 Low density of Conduction electrons

In the low-density regime of conduction electrons, the Kondo interaction has a pronounced effect on the magnetic phases of the system. Figure 18 illustrates the mean-field parameters as a function of temperature for different values of $J_K/|J_1|$

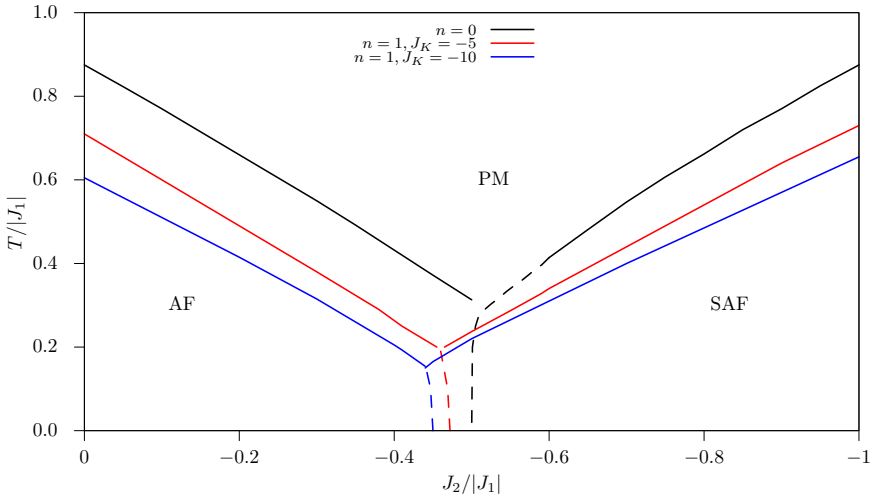

Figure 19 – Phase diagram of the $J_1 - J_2$ model with Kondo interaction at low conduction electron density ($n = 1$ and 0), showing the influence of Kondo coupling on magnetic phases.

for a fixed number of conduction electrons at two exchange interaction regimes: $J_2/|J_1|$= 0.00 and -1.00.

Figure 18 shows that the inclusion of Kondo interaction leads to a suppression of magnetic order, as evidenced by the reduction in critical temperatures for both AF and SAF phases. This effect is more pronounced at higher values of $J_K/|J_1|$ (blue line). Furthermore, the intensity of the mean fields is decreased as the Kondo interaction is enhanced. This effect becomes clear as $T/|J_1| \to 0$.

The axis on Figure 18 was inverted to better visualize the change in behavior of the disruption of magnetic order. In this case, it is observed that for $n = 1$ both $J_K/|J_1| = -5.0$ and -10.0 lead to a subtle, but noticeable "extra" decrease in mean field values of the SAF phase on the ground state ($T/|J_1| = 0.0$).

Figure 18 can help to build phase diagrams for the different regimes of Kondo interactions that are exhibited in Figure 19. The critical temperatures decrease as the intensity $J_K/|J_1|$ increases. In addition, the low-temperature AF/SAF phase transitions are also affected by the intensity of $J_K/|J_1|$. The AF/SAF first-order phase transitions take place at lower values of $|J_2/J_1|$ when $J_K/|J_1|$ increases its intensity. In this case, the SAF phase is favored at lower $|J_2/J_1|$ ratios, while the AF phase becomes less stable as the Kondo interaction strength increases. This

shift in phase boundaries highlights the complex interplay between magnetic interactions and Kondo screening in systems with low conduction electron density. This effect may reflect the enhancement of ferromagnetic correlations among localized spins induced by the Kondo interaction. As a consequence, the ferromagnetic stripes of localized spins can be slightly favored over the AF Néel ordering. These spin stripes can then help stabilize the SAF phase at the expense of the AF order.

Another important observation concerns the nature of the PM/SAF phase boundaries, which are characterized by the presence of a tricritical point where the transition changes from second-order to first-order. As the Kondo interaction strength increases, this point shifts to lower temperatures, as seen in Figure 19. This implies that the Kondo interaction affects the instability of thermal fluctuations associated with the highly competitive regions of the PM/SAF phase boundaries, leading to a change in the nature of the phase transition. Although the Kondo interaction cannot introduce a Kondo-singlet ground state at low electron density, it still strongly affects the phase transitions, namely in the highly frustrated regime.

5.2.2 High density of Conduction electrons

For high densities of conduction electrons, the Kondo interaction is able to establish a heavy fermion state on the system, even at $T = 0$. This is the main reason why the results obtained for this regime differ significantly from those observed in the low-density case.

A different behavior is observed at high electron density when compared to the previous case, as is evident in Fig. 20. The inclusion of more electrons under Kondo interaction significantly alters the magnetic phases and their transitions, particularly the region of strong frustration around $J_2/|J_1| \approx -0.5$.

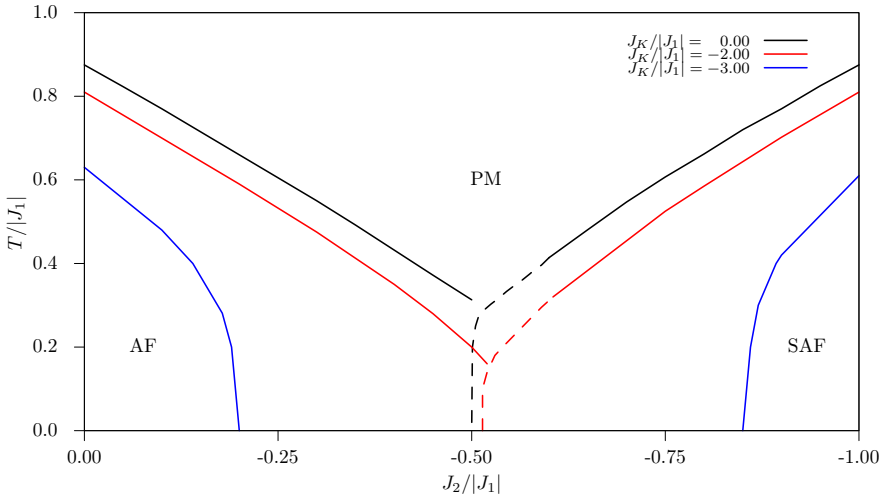

Figure 20 – Phase diagram of temperature versus the frustration parameter for the J_1–J_2 model with $n = 4$ and three values of the Kondo coupling: $J_k/|J_1| = 0.00$ (black curves), -2.00 (red curves), and -3.00 (blue curves). Solid lines represent second-order phase transitions, while dashed lines indicate first-order phase transitions.

In Figure 20, the presence of Kondo interactions not only suppresses the magnetic order, like in the case of one electron, but also leads to a shift in the phase boundaries in the opposite direction to that observed for $n = 1$. The SAF phase is slightly reduced, requiring a higher $|J_2/J_1|$ ratio for its stabilization, while the AF phase dominates the previous region of strong frustration when $J_K/|J_1| = -2.00$. This shift indicates that a weak Kondo coupling enhances the stability of the AF phase at the expense of the SAF phase. One of the reasons for this behavior is the overlap between the AF phase from the J_1-J_2 model and the AF phase induced by the Kondo interaction itself (Figure 8).

In contrast to the low-density case, at slightly higher intensities of $J_K/|J_1|$ (see blue curves of Figure 20), the tricritical point is no longer observed, and a new region of the phase diagram emerges when $n = 4$. This new region is characterized by the complete suppression of magnetic order, leading to a non-magnetic Kondo singlet state, as shown in Figure 20 for $J_k/|J_1| = -3.00$.

The presence of Kondo singlet formation is evident in the behavior of the spin correlation $\langle \mathbf{S}_i \mathbf{s}_i \rangle$, which tends to be -0.75. Figure 21 illustrates the evolution of

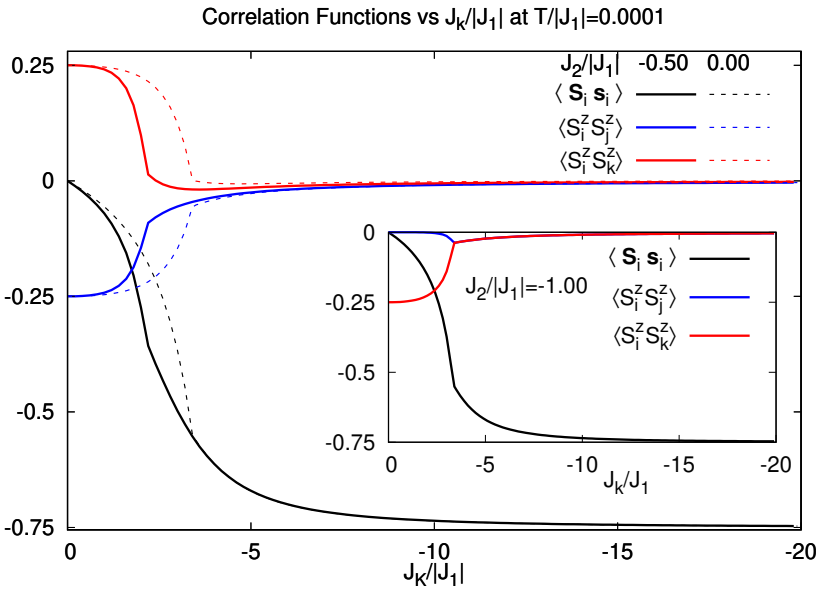

Figure 21 – Spin correlations between first-neighbor ($\langle S_i^z S_j^z \rangle$) and second-neighbor ($\langle S_i^z S_k^z \rangle$) localized moments, and between localized moments and conduction electrons ($\langle \mathbf{S}_i \mathbf{s}_i \rangle$), as a function of the Kondo interaction at $T/|J_1| = 0.0001$ with different values of $J_2/|J_1|$: 0.00 (dashed lines) and -0.50 (solid lines). The inset shows results for $J_2/|J_1| = -1.00$.

spin correlations between localized moments at $T/|J_1| = 0.0001$ [2]. For lower values of $J_K/|J_1|$ with $J_2/|J_1| = 0.00$ and -0.50, the system exhibits antiferromagnetic order, as indicated by $\langle S_i^z S_j^z \rangle \to -0.25$ and $\langle S_i^z S_k^z \rangle \to 0.25$.

In contrast, for higher intensities of $J_2/|J_1|$, the SAF order dominates the system: $\langle S_i^z S_j^z \rangle \to 0.00$ and $\langle S_i^z S_k^z \rangle \to -0.25$ (see the inset of Fig. 21). However, as $J_K/|J_1|$ increases, these correlations indicate that the long-range magnetic orders (AF and SAF) are suppressed, and the local correlation $\langle \mathbf{S}_i \cdot \mathbf{s}_i \rangle$ strengthens. In this regime, the Kondo interaction becomes dominant, leading to the formation of Kondo singlets, as indicated by $\langle \mathbf{S}_i \cdot \mathbf{s}_i \rangle \to -0.75$. Furthermore, Fig. 21 shows that magnetic correlations near the strong frustration regime (solid lines) are suppressed faster than the unfrustrated case (dashed lines) when the Kondo coupling increases.

To clarify the relationship between the non-magnetic phase and the Kondo coupling, Fig. 22 presents the correlations as a function of the frustration parameter

[2] This temperature value is assumed to be $0K$. This is done to avoid numerical instabilities at exactly zero temperature.

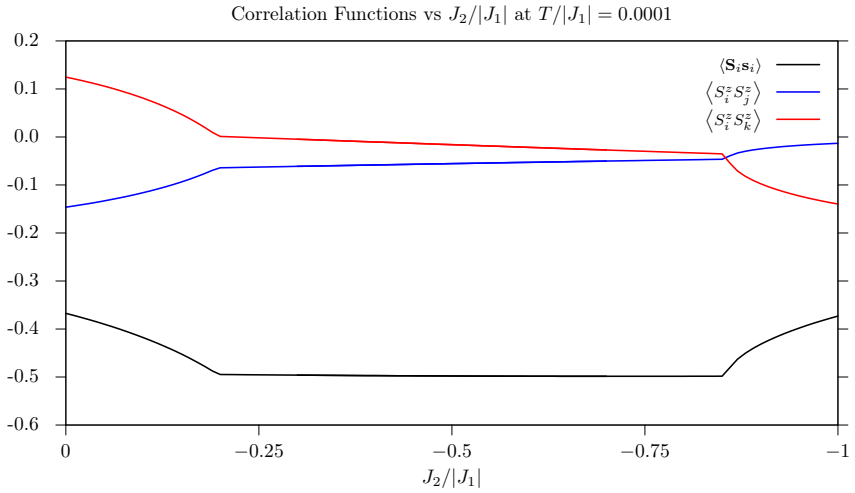

Figure 22 – Spin correlations between first-neighbor ($\langle S_i^z S_j^z \rangle$) and second-neighbor ($\langle S_i^z S_k^z \rangle$) localized moments, and between localized moments and conduction electrons ($\langle \mathbf{S}_i \mathbf{s}_i \rangle$), as a function of the exchange interaction $J_2/|J_1|$ for Kondo interaction $J_K/|J_1| = -3.0$ at $T/|J_1| = 0.0001$.

$J_2/|J_1|$ at a fixed $J_K/|J_1| = -3.0$ in the ground state. The AF spin-spin correlations decrease as $J_2/|J_1|$ introduces frustration into the system, as do the SAF correlations. In addition, the local correlation $\langle \mathbf{S}_i \cdot \mathbf{s}_i \rangle$ strengthens and maintains a nearly constant magnitude within the non-magnetic Kondo region.

These results show a clear formation of Kondo singlets with strong enough J_K interactions, which begins first in the highly frustrated region around $J_2/|J_1| \approx -0.5$, where the competition between magnetic interactions is maximum. However, as $J_2/|J_1|$ moves away from this critical region, the Kondo correlation decreases in strength, allowing magnetic order to re-emerge, as shown by the spin-spin correlations.

To explore the thermal effects on the spin-spin correlations, Fig. 23 presents $\langle S_i^z S_j^z \rangle$, $\langle S_i^z S_k^z \rangle$ and $\langle \mathbf{S}_i \mathbf{s}_i \rangle$ as a function of the temperature for the stronger frustrated regime when $J_K/|J_1| = -3.0$, -5.0 and 10. In this range of $J_K/|J_1|$, a non-magnetic phase is expected at low temperatures. The magnetic spin-spin correlations are away from the characteristic values for the AF and SAF ordered phases and tend to zero as both temperature and $J_K/|J_1|$ increase. On the other hand, the correlation $\langle \mathbf{S}_i \mathbf{s}_i \rangle$ is strongly affected by $J_K/|J_1|$, enhancing towards

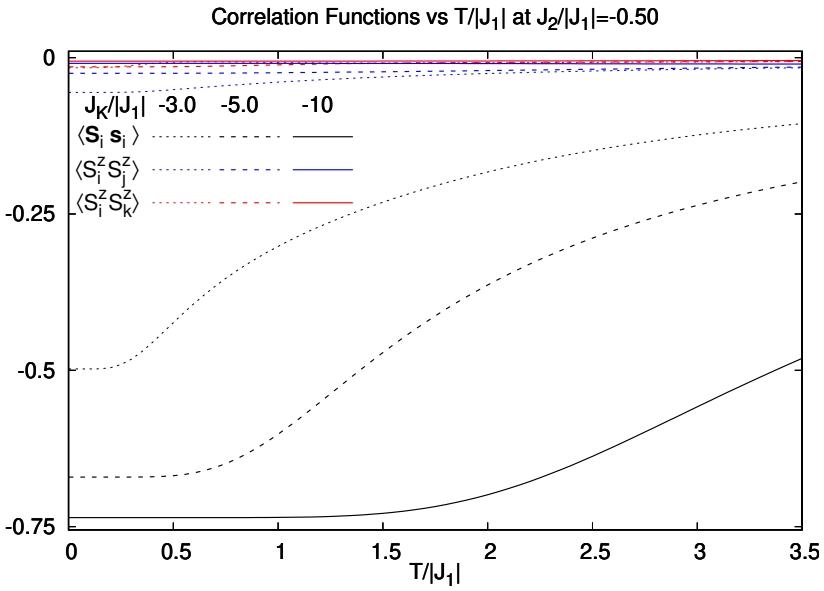

Figure 23 – Spin correlations $\langle S_i^z S_j^z \rangle$, $\langle S_i^z S_k^z \rangle$, and $\langle \mathbf{S}_i \mathbf{s}_i \rangle$) as a function of the temperature for $J_2/|J_1| = -0.50$ with different values of $J_K/|J_1|$: -3.00 (dotted lines), -5.00 (dashed lines), and -10 (solid lines).

-0.75 as $J_K/|J_1|$ increases. Increasing temperature suppresses the magnitude of this correlation, driving it to zero. It is important to remark that the temperature induces a change in the concavity of this correlation curve, indicating a disruption of singlet formation [39]. This behavior suggests that while the low-temperature regime is dominated by Kondo singlets, these singlets dissociate at higher temperatures as the system transitions into a canonical paramagnetic state.

To trace the boundaries of the Kondo (KO) state, the phase diagram of Figure 24 was constructed. This diagram shows the different phase boundaries between magnetic and non-magnetic states for temperature $T/|J_1| = 0.0001$. The AF order can be found at lower intensities of $J_2/|J_1|$ and can suffer a first-order transition to the SAF phase when the strength $J_2/|J_1|$ becomes dominant ($J_2/|J_1| \lesssim -0.5$). As the intensity of $J_K/|J_1|$ increases, the AF/SAF first-order transition boundary shifts slightly, favoring the AF order. However, for larger intensities of $J_K/|J_1|$, the Kondo state is observed. The AF/KO phase transitions are always second-order, indicating a quantum critical line. Conversely, the SAF/KO phase transition presents a more intricate physics. The transition is first-order in the vicinity of the highly frustrated regime, but evolves into a second-order transition for larger

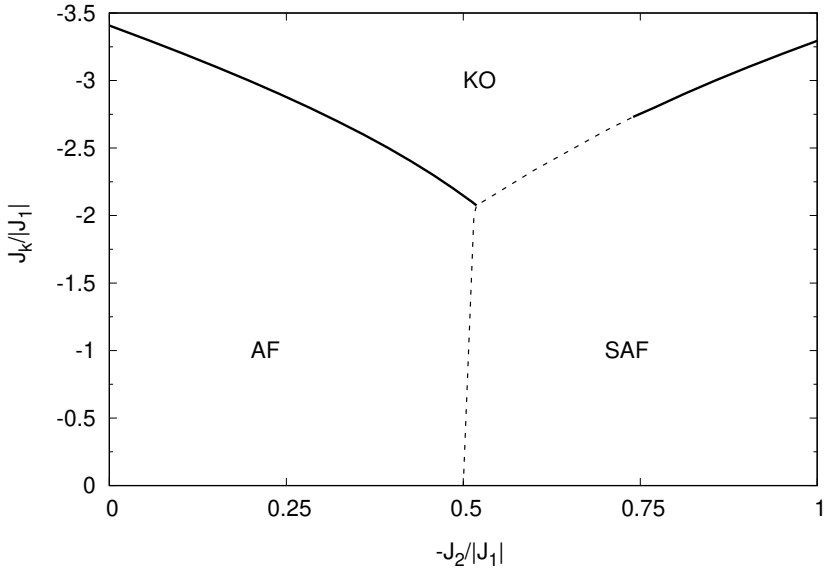

Figure 24 – Phase diagram of the $J_1 - J_2$ model with Kondo interactions at the ground state, showing the quantum boundaries between magnetic and non-magnetic phases. Solid and dashed lines represent second- and first-order phase transitions, respectively.

ratios of $J_2/|J_1|$. Consequently, the SAF/KO phase boundary features a quantum tricritical point.

The numerical results obtained via the Cluster Mean-Field (CMF) approach reveal a complex competition between geometric frustration and the Kondo effect. In the absence of Kondo coupling ($J_K = 0$), the benchmarked J_1-J_2 square lattice successfully recovers the transition from Néel antiferromagnetism to stripe antiferromagnetism near the critical ratio $J_2/|J_1| \approx -0.5$. Notably, the CMF method captures the suppression of the transition temperature in this regime, reflecting the heightened magnetic fluctuations inherent to the point of maximum frustration.

The introduction of the Kondo interaction J_K imposes a secondary tuning parameter on the system's ground state. As J_K increases, we observe a systematic degradation of the magnetic order parameters (m_{AF} and m_{SAF}). However, the resilience of these phases is highly dependent on the electronic filling n. In the low-density limit ($n = 1$), the scarcity of conduction electrons prevents efficient screening of the local moments, allowing magnetic order to persist even under significant Kondo coupling. Conversely, in the high-density limit ($n = 4$), the

abundance of carriers facilitates a robust Kondo singlet phase, leading to a rapid collapse of magnetic order and the emergence of a non-magnetic Heavy Fermi Liquid state. This density-dependent suppression highlights that the "Doniach competition" is not merely a function of coupling strength, but is fundamentally constrained by the available carrier density in the conduction band.

6 Conclusions

This dissertation provided a detailed investigation into the magnetic phase stability of the frustrated J_1-J_2 Kondo Lattice Model. By employing the Cluster Mean-Field approximation on a 2×2 cluster, we successfully accounted for the short-range correlations and quantum fluctuations that are typically neglected in single-site treatments. The primary conclusions of this study are summarized as follows:

- **Destabilization of Magnetic Order:** We have demonstrated that exchange frustration and the Kondo effect act as complementary mechanisms in the suppression of long-range order. While the competition between J_1 and J_2 exchange interactions weakens the magnetic resilience of the square lattice (particularly near the $J_2/|J_1| \approx -t70.5$ regime), the Kondo coupling J_K provides the electronic channel for local moment screening. This synergy effectively lowers the critical energy threshold required for the system to undergo a transition from an ordered magnetic state to a non-magnetic Kondo singlet state.

- **Density-Dependent Phase Stability:** We demonstrated that the stability of the AF and SAF phases is critically linked to the conduction electron density (n). In high-density regimes, the abundance of carriers facilitates a robust Kondo Singlet phase. Conversely, in low-density limits, the system exhibits a marked resilience of magnetic order, as the scarcity of conduction electrons prevents the total screening of local moments, even under significant Kondo coupling.

- **Nature of Transitions:** Our analysis of the Helmholtz free energy reveals that the first-order (discontinuous) nature of the phase transitions is intimately tied to the frustration and the Kondo scale. While the transition from the SAF phase is characteristically first-order in the pure exchange limit ($J_K = 0$) and under high Kondo coupling, we observe that lower electron densities tend to vanish these first-order boundaries. This suggests that the

conduction electron filling is a key parameter not only for the stability of the phases but also for the thermodynamic nature of the quantum phase transitions in frustrated systems.

From a Materials Science perspective, these findings offer theoretical guidance for the development of heavy-fermion materials. By tuning both the lattice frustration (via chemical substitution or epitaxial strain) and the carrier concentration (via doping), it may be possible to precisely control the quantum critical regions of these systems. Future research should expand the cluster dimensions to further explore the possibility of a Spin Liquid phase in the region of maximum frustration and investigate the impact of anisotropic exchange interactions on the resulting phase diagram.

Referências

1 COEY, J. M. D. **Magnetism and Magnetic Materials**. Cambridge New York: Cambridge University Press, 2009. ISBN 978-0-511-67743-4 978-0-511-68515-6 978-0-511-68192-9 978-0-511-67994-0 978-0-511-84500-0.

2 ZHOU, R.; ZHANG, X.; LI, G. **Doniach Phase Diagram for Kondo Lattice Model on the Square and Triangular Lattices**. [S.l.]: arXiv, 2023.

3 URAGA, S.; TADA, Y. Spin nematic order and superconductivity in J1-J2 Kondo lattice model on the. **Physical Review B**, jan. 2025.

4 ALEXANDRADINATA, A. *et al.* The future of the correlated electron problem. **SciPost Physics Community Reports**, p. 8, jun. 2025.

5 FUMEGA, A. O.; LADO, J. L. Nature of the Unconventional Heavy-Fermion Kondo State in Monolayer CeSiI. **Nano Letters**, v. 24, n. 14, p. 4272–4278, abr. 2024. ISSN 1530-6984, 1530-6992.

6 COLEMAN, P. **Introduction to Many-Body Physics**. Cambridge: Cambridge University Press, 2015. ISBN 978-1-139-02091-6.

7 WIESER, R. Cluster mean-field theory studies of the frustrated two-dimensional quantum-mechanical J 1 - J 2 Heisenberg model. **Annals of Physics**, v. 427, p. 168414, abr. 2021. ISSN 00034916.

8 REN, Y.-Z.; TONG, N.-H.; XIE, X.-C. Cluster mean-field theory study of J_1 -J_2 Heisenberg model on a square lattice. **Journal of Physics: Condensed Matter**, v. 26, n. 11, p. 115601, mar. 2014. ISSN 0953-8984, 1361-648X.

9 ASHCROFT, N. W.; MERMIN, N. D. **Solid State Physics**. New York: Holt, Rinehart and Winston, 1976. ISBN 978-0-03-083993-1.

10 KITTEL, C. **Introduction to Solid State Physics**. 8th ed. ed. New York: J. Wiley & sons, 2005. ISBN 978-0-471-68057-4.

11 JACKSON, J. D. **Classical Electrodynamics**. 3. ed., [nachdr.]. ed. Hoboken, NY: Wiley, 2009. ISBN 978-0-471-30932-1.

12 LANDAU, L. D.; LIFŠIC, E. M. **Statistical Physics.** 3rd ed., revised and enlarged. ed. Amsterdam: Butterworth-Heinemann, an imprint of Elsevier, 2022. ISBN 978-81-8147-790-3.

13 RUDERMAN, M. A.; KITTEL, C. Indirect Exchange Coupling of Nuclear Magnetic Moments by Conduction Electrons. **Physical Review**, American Physical Society (APS), v. 96, n. 1, p. 99–102, out. 1954. ISSN 0031-899X.

14 KASUYA, T. A Theory of Metallic Ferro- and Antiferromagnetism on Zener's Model. **Progress of Theoretical Physics**, Oxford University Press (OUP), v. 16, n. 1, p. 45–57, jul. 1956. ISSN 0033-068X.

15 YOSIDA, K. Magnetic Properties of Cu-Mn Alloys. **Physical Review**, American Physical Society (APS), v. 106, n. 5, p. 893–898, jun. 1957. ISSN 0031-899X.

16 BLUNDELL, S. **Magnetism in Condensed Matter**. Oxford ; New York: Oxford University Press, 2001. (Oxford Master Series in Condensed Matter Physics). ISBN 978-0-19-850592-1.

17 ONSAGER, L. Crystal Statistics. I. A Two-Dimensional Model with an Order-Disorder Transition. **Physical Review**, v. 65, n. 3-4, p. 117–149, fev. 1944. ISSN 0031-899X.

18 MERMIN, N. D.; WAGNER, H. Absence of Ferromagnetism or Antiferromagnetism in One- or Two-Dimensional Isotropic Heisenberg Models. **Physical Review Letters**, v. 17, n. 22, p. 1133–1136, nov. 1966. ISSN 0031-9007.

19 SAKURAI, J. J.; NAPOLITANO, J. **Modern Quantum Mechanics**. Third edition. Cambridge: Cambridge University Press, 2021. ISBN 978-1-108-47322-4.

20 EISBERG, R. M.; RESNICK, R. **Fisica quantica: atomos, moleculas, solidos, nucleos e particulas**. Rio de Janeiro (RJ): Campus, 1994. ISBN 978-85-7001-309-5.

21 LI, S.-W.; JIANG, F.-J. A comprehensive study of the phase transitions of the frustrated J1-J2 Ising model on the square lattice. **Progress of Theoretical and Experimental Physics**, abr. 2024.

22 CASTELNOVO, C.; MOESSNER, R.; SONDHI, S. L. Magnetic monopoles in spin ice. **Nature**, v. 451, n. 7174, p. 42–45, jan. 2008. ISSN 0028-0836, 1476-4687.

23 SCHOLLWöCK, U.; RICHTER, J.; FARNELL, D. J. J.; BISHOP, R. F. (Ed.). **Quantum Magnetism**. Berlin, Heidelberg: Springer Berlin Heidelberg, 2004. v. 645. (Lecture Notes in Physics, v. 645). ISBN 978-3-540-21422-9 978-3-540-40066-0. Disponível em: ⟨http://link.springer.com/10.1007/b96825⟩.

24 SAVARY, L.; BALENTS, L. Quantum spin liquids: A review. **Reports on Progress in Physics**, v. 80, n. 1, p. 016502, jan. 2017. ISSN 0034-4885, 1361-6633.

25 GRIFFITHS, D. J. **Introduction to Electrodynamics**. 3rd ed. ed. Upper Saddle River, N.J: Prentice Hall, 1999. ISBN 978-0-13-805326-0.

26 MEISSNER, W.; VOIGT, B. Messungen mit Hilfe von flüssigem Helium XI Widerstand der reinen Metalle in tiefen Temperaturen. **Annalen der Physik**, v. 399, n. 7, p. 761–797, jan. 1930. ISSN 0003-3804, 1521-3889.

27 HAAS, W. D.; BOER, J. D.; BERG, G. V. D. The electrical resistance of gold, copper and lead at low temperatures. **Physica**, v. 1, n. 7-12, p. 1115–1124, maio 1934. ISSN 00318914.

28 KONDO, J. Resistance Minimum in Dilute Magnetic Alloys. **Progress of Theoretical Physics**, v. 32, n. 1, p. 37–49, jul. 1964. ISSN 0033-068X, 1347-4081.

29 DONIACH, S. The Kondo lattice and weak antiferromagnetism. **Physica B+C**, v. 91, p. 231–234, jul. 1977. ISSN 03784363.

30 GEGENWART, P.; SI, Q.; STEGLICH, F. Quantum criticality in heavy-fermion metals. **Nature Physics**, v. 4, n. 3, p. 186–197, mar. 2008. ISSN 1745-2473, 1745-2481.

31 CHEN, R. Y.; WANG, N. L. Infrared properties of heavy fermions: Evolution from weak to strong hybridizations. **Reports on Progress in Physics**, v. 79, n. 6, p. 064502, jun. 2016. ISSN 0034-4885, 1361-6633.

32 KAVAI, M. *et al.* Inhomogeneous Kondo-lattice in geometrically frustrated Pr2Ir2O7. **Nature Communications**, v. 12, n. 1, p. 1377, mar. 2021. ISSN 2041-1723.

33 YAMAMOTO, D. Correlated cluster mean-field theory for spin systems. **Physical Review B**, v. 79, n. 14, p. 144427, abr. 2009. ISSN 1098-0121, 1550-235X.

34 QIAN, X.; QIN, M. Absence of spin liquid phase in the J_1-J_2 Heisenberg model on the square lattice. **Physical Review B**, v. 109, n. 16, p. L161103, abr. 2024. ISSN 2469-9950, 2469-9969.

35 METCALF, M.; REID, J. K.; COHEN, M.; BADER, R. **Modern Fortran Explained: Incorporating Fortran 2023**. [new] edition. Oxford: Oxford

University Press, 2023. (Numerical Mathematics and Scientific Computation). ISBN 978-0-19-198794-6.

36 WILLIAMS, T. *et al.* **Gnuplot 6.0: An Interactive Plotting Program**. 2024.

37 JIN, S.; SEN, A.; GUO, W.; SANDVIK, A. W. Phase transitions in the frustrated Ising model on the square lattice. **Physical Review B**, v. 87, n. 14, p. 144406, abr. 2013. ISSN 1098-0121, 1550-235X.

38 KALZ, A.; HONECKER, A.; FUCHS, S.; PRUSCHKE, T. Phase diagram of the Ising square lattice with competing interactions. **The European Physical Journal B**, v. 65, n. 4, p. 533–537, out. 2008. ISSN 1434-6028, 1434-6036.

39 ZLATIC, V.; AVIANI, I. **The Phase Diagram of Heavy Fermions with Cerium and Europium Ions**. [S.l.]: arXiv, 2023.